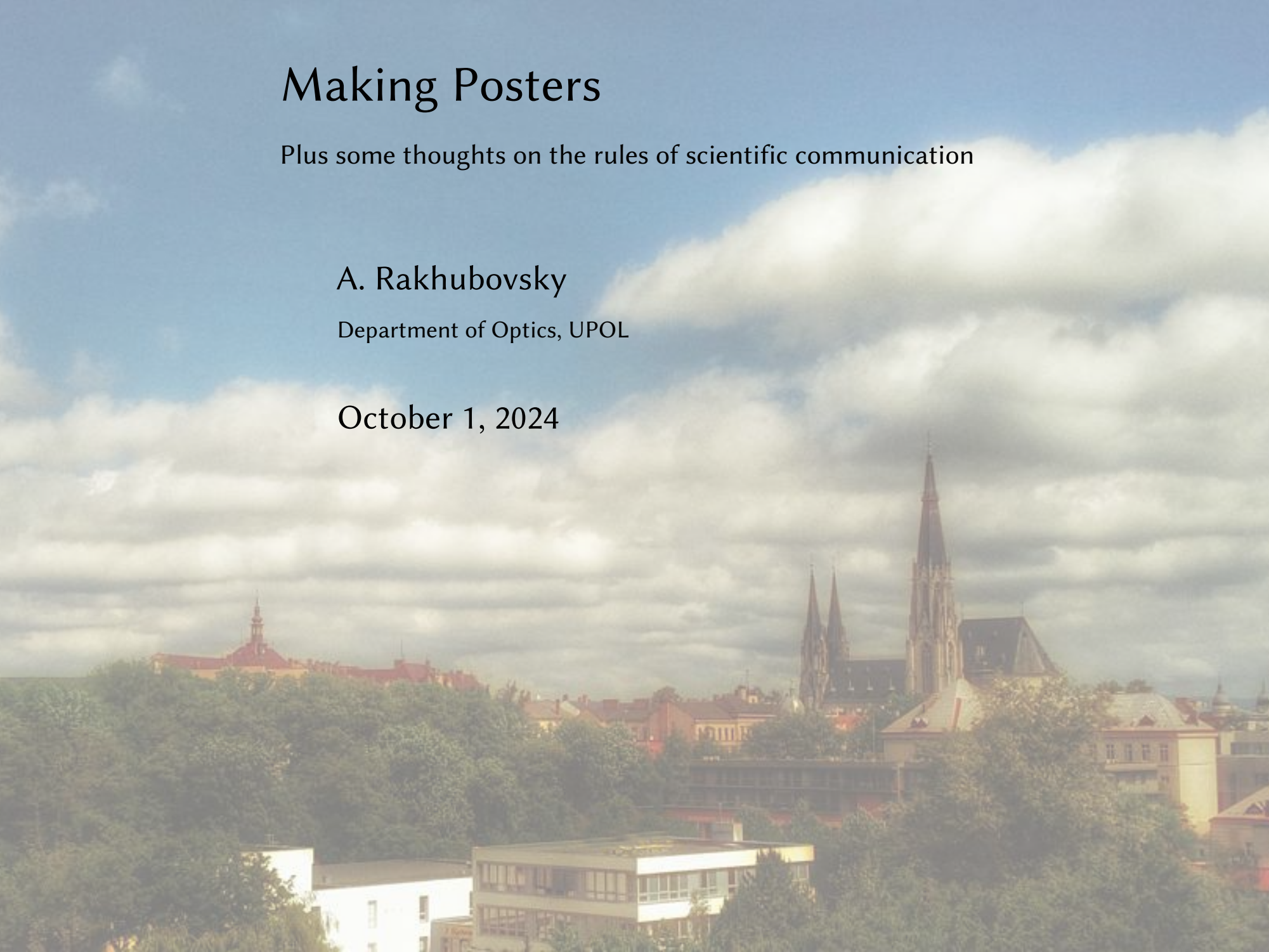

Making Posters

Plus some thoughts on the rules of scientific communication

A. Rakhubovsky

Department of Optics, UPOL

October 1, 2024

Introduction: Presentation of Your Research

Planning a Poster

Implementing a Poster: Typography and Technical Details

Conclusions

Please Interrupt!

bit.ly/upol-posters

Outline

bit.ly/upol-posters

What we expect

bit.ly/upol-posters

What we get

bit.ly/upol-posters

What we get

bit.ly/upol-posters

What we get

bit.ly/upol-posters

What we get

bit.ly/upol-posters

What we get

Last two pics: Google "AGU (Americal Geophysical Union) Meeting"

bit.ly/upol-posters

What we get

bit.ly/upol-posters

Posters for different purposes

Poster that hangs on a wall

bit.ly/upol-posters

Posters for different purposes

Poster that hangs on a wall

Poster that you hang out next to

Image source: Wikipedia "Poster Session"

bit.ly/upol-posters

DALL-E: 'research institute corridor with scientific posters on the walls'

bit.ly/upol-posters

DALL-E: 'research institute corridor with scientific posters on the walls'

bit.ly/upol-posters

DALL-E: 'research institute corridor with scientific posters on the walls'

bit.ly/upol-posters

DALL-E: 'research institute corridor with scientific posters on the walls'

bit.ly/upol-posters

Our goal poster

bit.ly/upol-posters

Main Misconception About the Conference Posters

No one reads them

bit.ly/upol-posters

The Plan of the Presentation

Grab the attention

Try to not lose the attention

The Plan of the Presentation

Grab the attention

- Interesting title
- Large and nice figures

Try to not lose the attention

bit.ly/upol-posters

The Plan of the Presentation

Grab the attention

- Interesting title
- Large and nice figures

Try to not lose the attention

- Keep things simple

bit.ly/upol-posters

The Plan of the Presentation

Grab the attention

- Interesting title
- Large and nice figures

Try to not lose the attention

- Keep things simple

Prepare different level of details

- A few sentences summary
- “Elevator talk” — presentation in three minutes
- …
- The full talk

bit.ly/upol-posters

The Plan of the Presentation

Grab the attention

- Interesting title
- Large and nice figures

Try to not lose the attention

- Keep things simple

Prepare different level of details

- A few sentences summary
- “Elevator talk” — presentation in three minutes
- …
- The full talk

This is difficult

Seriously

bit.ly/upol-posters

Outline

bit.ly/upol-posters

Structure of Research/ The Problem

Problem

bit.ly/upol-posters

Structure of Research/ The Problem

?

Knowledge Before

Problem

bit.ly/upol-posters

Structure of Research/ The Problem

?

Problem

Knowledge Before

+

Tools

Structure of Research/ The Problem

?

Problem

Knowledge Before

+

Tools

=

Knowledge After

Practical Steps

Pick contents

- Determine the main contribution
- Write it down in 3 sentences + 1 figure
- Prepare supporting data (definitions + graphs)

Sketch (pen + paper)

- Make a few (2-4) sketches with different layout

Implement

- Decide the tools (programs)
- Choose the looks (fonts + colors)

bit.ly/upol-posters

Example Structure

PHYSICAL REVIEW A 91, 062317 (2015)

Robust entanglement with a thermal mechanical oscillator

Andrey A. Rakhubovsky* and Radim Filip
Department of Optics, Palacký University, 17. listopadu 1192/12, 771 46 Olomouc, Czech Republic
(Received 14 January 2015; published 15 June 2015)

We consider a protocol to entangle an electromagnetic pulse with a mechanical oscillator at high temperature. We show this protocol to be capable of entangling currently existing experimental systems at relatively high (above the available cryostat) temperatures of the mechanical part. We also predict a possibility of conditional squeezing of the mechanical mode below the shot noise level at the cryostat temperatures.

DOI: 10.1103/PhysRevA.91.062317 PACS number(s): 03.67.Bg, 42.50.Wk, 42.50.Ex, 42.50.Dv

I. INTRODUCTION

Quantum optomechanics is a rapidly developing field of quantum physics with continuous variables profiting from the new possibilities of quantum control of mechanical oscillators [1–4]. This hybrid experimental platform directly links the quantum properties of light and microwave radiation, represented by the model of a linear oscillator, with the characteristics of real mechanical-type oscillator. These quantum mechanical oscillators have physical features and capabilities that distinguish them from the properties of light, many times examined in details in continuous-variable quantum optics [5–7]. Mechanical vibration of the real position of the oscillator naturally allows the bridge to thermodynamics and recently ongoing examination of quantum thermodynamics with mechanical oscillators [8–10]. Thinking about this direction at a very basic level, we first admit that the mechanical oscillator is an open system. It naturally tends to thermodynamic equilibrium with its thermal environment. Second, quantum optomechanics can advantageously exploit radiation pressure to push the mechanical oscillators out of thermodynamic equilibrium and, therefore, it allows us to generate interesting quantum effects.

Continuous-variable quantum entanglement [5] is a basic phenomenon demonstrating the connection between light and mechanical oscillator out of thermal equilibrium. Theoretically, an interaction caused by radiation pressure allows the entangling process of amplification of mechanical vibration and radiation at the same time [2]. In quantum optics, such amplification processes in nonlinear crystals lead to the generation of squeezed states of light and Gaussian entanglement between optical beams [7]. These are useful resources for a variety of operations developed in quantum optics and quantum information processing [7,11,12]. In quantum optics, it is easy to achieve the ground state of the mode of light modeled by the linear harmonic oscillator since the light interacts very weakly with matter and the modes can be easily blocked. On the other hand, the mechanical oscillators are inherently thermally occupied by phonons and their cooling is necessary by use of sophisticated techniques [4]. For the intensively cooled electromechanical oscillators, Gaussian quantum entanglement has been recently experimentally demonstrated in the pulsed regime [13]. At the same time, it was theoretically predicted that Gaussian quantum entanglement is observable at the output of the amplification process for thermal-equilibrium input states with arbitrary temperature [14]. These methods could, in principle, generate *thermal* entanglement without any cooling mechanical oscillators and also the mechanical squeezed state of the mechanical oscillator. Such thermal entanglement does not naturally occur in optical nonlinear processes, so this type of thermal Gaussian entanglement has not been studied in quantum optics. In pulsed quantum optomechanics it is possible to achieve an ideal amplification regime approximated by an adiabatic elimination of the optical mode when the mechanical oscillator is not much thermally occupied [15–17]. Unfortunately, this approximation is generally not applicable for an interesting case of extreme temperatures of the mechanical oscillator, where thermal entanglement can still be surprisingly detected.

In this paper, the pulsed generation of thermal entanglement between light and mechanical oscillator is analyzed without using the adiabatic approximation. The bound on generation of the entanglement is defined in the limit of the large temperature of the mechanical oscillator. Generation of thermal entanglement is analyzed for the current electromechanical experiment [13] and subsequently for the future optomechanical experiment [18]. For both types of experiments, existence and robustness of the thermal Gaussian entanglement is confirmed for the large number $n_{th} \approx 400$ of thermal quanta for the experiment in [13] and $n_{th} \approx 240$ for the experiment in [18]. In addition, it is shown that thermal entanglement allows

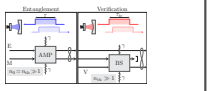

FIG. 1. (Color online) Protocol to create and verify entanglement. First the blue-detuned entangling pulse with length τ enters the cavity, then after the delay time τ_{del} the red-detuned pulse lasting τ_0 performs the read-out of the state of the mechanical subsystem. Mechanical system is initially in a thermal state with occupation n_0 and is coupled at the rate γ to the thermal bath with occupation n_{th}.

*andrey.rakhubovsky@upol.cz

TABLE I. Values of parameters used for numerical estimations.

Quantity	Palomaki *et al.* [13]	Chan *et al.* [18]
Mechanical frequency ω	$2\pi \times 10.34$ MHz	$2\pi \times 3.9$ GHz
Viscous damping rate γ	$2\pi \times 35$ Hz	$2\pi \times 39$ kHz
Cavity half width κ	$2\pi \times 180$ kHz	$2\pi \times 0.25$ GHz
Sideband resolution parameter κ/ω	0.02	0.06
Single-photon coupling g_0	$2\pi \times 200$ Hz	$2\pi \times 0.9$ MHz
Photon number $n_{cav} \approx n_{cav,B}$	$2\delta \times 10^3$	1.5×10^3
Enhanced coupling $g_B = g_R$	$2\pi \times 30.9$ kHz	$2\pi \times 35.0$ kHz
Coupling $G_R \equiv G_B \equiv G_0$	$2\pi \times 5.3$ kHz	$2\pi \times 9.8$ kHz
Duration of entangling pulse τ	35 μs	0.13 μs
Time span between the pulses $\tau_{del}^{(0)}$	10 μs	0.04 μs
Duration of the verification pulse τ_0	30 τ	30 τ

to underestimation of entanglement in case the state being analyzed is asymmetric (i.e., variances of one of the modes are exceedingly higher than those of the another). According to the recent research [14] this is the very case of the optomechanical entanglement particularly at the relatively high (above the available cryostat) temperatures of the mechanical part. We also predict a possibility of conditional squeezing of the mechanical mode below the shot noise level at the cryostat temperatures.

In [13] the entanglement was authenticated by analysis of the covariance matrix between the quadratures of the entangling pulse and the verification pulse. These quantities following the considerations of [15] were defined by projection of the leaking field quadratures $u^{out} = (X^{out}, Y^{out})$ on the exponential envelopes. Explicitly this projection reads

$$U^R = C_R \int_{t_{in}}^{t_{fin}} dt\, e^{\kappa t} u(t) e^{i\omega t}, \quad U^B = C_B \int_{t_{in}}^{t_{fin}} dt\, e^{\kappa t} u(t) e^{-i\omega t}. \tag{6}$$

The integration is done over the duration of corresponding pulse denoted as $T_{R,B}$; $C_{I,R}$ is the normalizing coefficient, so $\langle U_i^I U_i^I \rangle = 1$, where $k = I, R, B$. The exponential rates are defined as $\tilde{G}_k = g_0^2/\kappa$.

The quadratures of the leaking field are computed using the usual input-output relations [32],

$$u_j^{out}(t) = \sqrt{2\kappa}\, a_j(t) - u_j^{in}(t), \quad j = 1, 2. \tag{7}$$

Here $u^{in} = (X^{in}, Y^{in})$ denotes the vector of quadratures of the input field. Please note that both u^{out} and u^{in} are two-dimensional vectors so only the first two components of u are used.

Using the definitions given one can make estimations for the covariance matrix of the quadratures of the two pulses. The matrix is written as follows with the help of 2×2 blocks that contain autocorrelations of and cross correlations between the two pulses,

$$\mathbb{V}_\eta = \begin{pmatrix} \langle U_i^R U_j^R \rangle & \langle U_i^R U_j^B \rangle \\ \langle U_i^B U_j^R \rangle & \langle U_i^B U_j^B \rangle \end{pmatrix}, \quad i, j = 1, 2.$$

To compute the elements of $\mathbb{V}_\eta$ we use the same approach. We substitute the formal solution (5) and the definition of pulse quadratures (6) into the input-output relations (7). After swapping the order of the averaging over state and of the integration over time we are able to relate $\mathbb{V}_\eta$ with the covariance matrix $\mathbb{V}_0$ of the initial state of the system and the correlations of the Langevin forces.

In more details, for instance, for $\langle U_i^R U_j^R \rangle$ one can obtain

$$\begin{aligned} \langle U_i^R U_j^R \rangle = C_R^2 \Big[& \int_0^\tau \int_0^\tau d\alpha\, d\alpha'\, e^{\kappa(\alpha+\alpha')} \times 2\kappa \Big[M(\alpha) \mathbb{V}_0 M^\top(\alpha') \\ & + \int_0^\alpha d\alpha \int_0^{\alpha'} d\alpha'\, M(\alpha - \alpha') \bar{F} (\alpha - \alpha') M^\top(\alpha' - \alpha') \\ & - \int_0^\alpha d\alpha\, M(\alpha - \alpha') \bar{F}(\alpha - \alpha') \\ & - \int_0^{\alpha'} d\alpha' \bar{F}(\alpha' - \alpha) M^\top(\alpha' - \alpha') \\ & + \frac{1}{2\kappa} \bar{F}(\alpha - \alpha') \Big]_{ij}, \\ & i, j = 1, 2. \end{aligned}$$

In this equation we introduced a new matrix $\bar{F}$ characterizing correlations between the intracavity Langevin forces (elements of f) and the quadratures of incident field u^{in}, namely,

$$\langle \bar{F}(\alpha - s')_{ij} = [u^{in}(s) \otimes u^{in}(s')] = \mathrm{diag}\left[\tfrac{1}{2}, \tfrac{1}{2}, 0, 0\right] \delta(\alpha - s').$$

The mechanical subsystem is assumed to be initially in a thermal state with occupation number n_{th} and the mode of the cavity is assumed to be in vacuum, so the covariance matrix of the initial state is as follows:

$$\mathbb{V}_0 = \mathrm{diag}\left[\tfrac{1}{2}, \tfrac{1}{2}, n_0 + \tfrac{1}{2}, n_0 + \tfrac{1}{2}\right].$$

V. RESULTS OF COMPUTATION

A. Verification of entanglement

To prove the validity of our method we first compare the results we obtain with the experimental ones reported in Ref. [13], namely we estimate the covariance matrix of the two consequent pulses (the entangling and verification ones) for the same experimental setup.

The result of numerical analysis is presented in Fig. 2(a) (for the exact values of parameters we used for estimations please see Table I). There is the figure representation of the elements of the covariance matrix of the quadratures of two pulses for a pre-cooled close to the ground-state mechanical oscillator in a cryogenic bath ($n_0 = 0$, $n_{th} = 40$). Empty bars correspond to the elements obtained in the case of perfect detection ($\eta = 1$) and solid bars correspond to attenuation in both modes $\eta = 0.2$. We see here a good quantitative coincidence with the reported experimental results.

The figure contains two pairs of traces of logarithmic negativity between the two pulses versus the mechanical occupation. The initial occupation n_0 of the mechanical mode along the traces is assumed to be equal to the occupation n_{th} of the mechanical bath (the mechanical mode is assumed to be at equilibrium state with its environment).

The darker curves employ the parameters reported in Ref. [13]. The logarithmic negativity is computed under the assumption of perfect detectors and absence of losses (dashed line) and under the realistic assumption of damping in both modes with effective transmittance $\eta = 0.2$ (solid line) due to nonperfect detectors.

It is clear from the figure that the entanglement between the pulses is robust against temperature of the mechanical environment which proves the pre-cooling stage is unnecessary in the entangling protocol for the maximum temperature allowing entanglement is ~65 mK, about three times higher than the temperature of the cryostat). Comparison of the traces demonstrates that the damping in both modes does not completely destroy the entanglement but only decreases its value, i.e., the entanglement is robust against attenuation in both modes. It is a clear witness that the robust version of thermal entanglement predicted in [14] can be observed in recent experiment [13].

The two steeper (lighter) curves in Fig. 2(a) represent logarithmic negativity computed for the same protocol within the optomechanical crystal experimental setup reported in Ref. [18]. Although the phonon number boundary is lower in this case, one should note that the frequency of the mechanical mode is several orders higher in this experiment and owing to this the boundary temperature is actually higher (more than 40 K, twice as high as the temperature of the corresponding cryostat, 20 K).

It needs to be underlined that the negativity estimated in Fig. 2(a) is the measure of entanglement between the two

particular type of interaction can be deduced from the general form [13,28],

$$A = \begin{pmatrix} -\kappa & 0 & g_R & g_B \\ 0 & -\kappa & -g_B & -g_R \\ g_R & g_B & -\gamma/2 & 0 \\ -g_B & -g_R & 0 & -\gamma/2 \end{pmatrix}$$

by equating $g_R = 0$ for the blue detuned pulse, $g_B = 0$ for the red detuned pulse or both $g_R = g_B \equiv 0$ for the free evolution between the pulses ($g_{R,B}$ denote the optomechanical coupling enhanced by a number of intracavity photons in the corresponding pulse; $g_{\circ} \equiv g_0\sqrt{n_{cav}}$, $k = B, R$).

The system under consideration is initially in a Gaussian state and the linear dynamics preserves this quality. So the correlation properties of the system can be completely characterized by its two first moments, of which we are interested in second ones, namely the covariance matrix (CM) with elements defined as

$$V_{ij}(t) = \langle u_i(t) \circ u_j(t) \rangle. \tag{4}$$

To estimate it we use the approach similar to the one of Refs. [30,31]. The solution of the equations of motion could be formally written in the form,

$$u(t) = M(t - t_0) u(t_0) + \int_{t_0}^{t} ds M(t - s) f(s), \tag{5}$$

where M is the matrix exponential $M(t) \equiv \exp(At)$. Performing substitution of the equation above into the definition of elements of the CM and integrating the order of integration and averaging one can obtain the expression for the covariance matrix of the intracavity quadratures:

$$\begin{aligned} V(t) = {} & M(t - t_0) V(t_0) M^\top (t - t_0) \\ & + \int_{t_0}^{t} ds\, M(t - s) F M^\top (t - s), \end{aligned}$$

where $^\top$ stands for transposition, F is a matrix of correlations between the Langevin forces:

$$\begin{aligned} \langle f_i(s) \circ f_j(s') \rangle \equiv {} & F \delta(s - s') \\ = {} & \mathrm{diag}\left[\kappa, \kappa, \gamma\left(n_{th} + \tfrac{1}{2}\right), \gamma\left(n_{th} + \tfrac{1}{2}\right)\right] \delta(s - s'). \end{aligned}$$

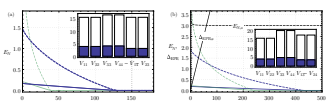

FIG. 2. (Color online) Different types of entanglement (logarithmic negativity) versus the temperature (occupation number) of the mechanical subsystem. (a) Entanglement between the quadratures of the entangling and the verification pulses. (b) Entanglement between the entangling pulse and the mechanical mode. Darker (blue) traces, electromechanical experimental setup reported by Palomaki *et al.* [13]; lighter (green) traces, optomechanical crystal by Chan *et al.* [18]. Dashed lines, lossless case; solid lines, realistic damping in both modes, $\eta = 0.2$. (Inset) Nonzero elements of covariance matrix simulating the experiment from Ref. [13] (initial mechanical occupation $n_0 = 0$, mechanical bath occupation $n_{th} = 40$). Black lines in (b) represent logarithmic negativity $E_{N,a}$ and EPR variance $\Delta_{EPR,a}$ of the optomechanical system calculated after the adiabatic elimination of the cavity mode. For the parameters utilized for estimations see Table I.

pulses emerging from the cavity but not between field and matter although the entanglement is created by means of optomechanical interaction.

It is also illustrative to check how the entanglement between the pulses can tolerate longer separations between the pulses. The dependence of the logarithmic negativity on the time separation of the pulses (in units of $\tau_{del}^{(0)}$ used to plot Fig. 2) is presented in Fig. 3. It shows, for instance, that the entanglement between the two pulses can persist even when the time span between them is twice as long as the duration of the entangling pulse.

B. Optomechanical entanglement

Another figure of merit is the optomechanical entanglement between the motion of the mechanical subsystem and the quadratures of the leaking field immediately after the entangling pulse. This entanglement exhibits even stronger robustness against the noisy thermal bath of the mechanical mode. The traces of logarithmic negativity versus the mechanical occupation are presented in Fig. 2(b).

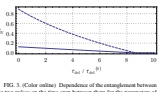

FIG. 3. (Color online) Dependence of the entanglement between the two pulses on the time span between them for the parameters of experiment by Palomaki *et al.* [13]. Dashed and solid lines correspond to the lossless case and the case of losses $\eta = 0.2$, respectively.

The two pairs of lighter curves represent the logarithmic negativity estimated using our approach versus the mechanical occupation for Refs. [13] and [18]. The optomechanical entanglement in this setup appears to be robust to both the temperature of the mechanical bath and the initial temperature of mechanical mode as well as robust to attenuation in both the mechanical and optical modes.

In the inset to Fig. 2(b) one can see the visualization of nonzero elements of the covariance matrix between the blue pulse and the mechanical mode after the (entangling) interaction is complete. Comparison of this covariance matrix with one of the two pulses reveals that the verification (red detuned) pulse does indeed perform state transfer from the mechanical mode to the leaking field with efficiency close to the ratio κ_{ext}/κ of two decay rates: the one due to the coupling of the circuit to the transmission line and the total decay rate of the circuit. The residual discrepancy is caused by the mechanical decoherence taking place during the interval between the pulses.

Due to the nonzero temperature of the mechanical bath ($n_{th} \neq 0$) the optomechanical state is asymmetrical even though the initial occupation of the mechanical mode was equal to zero ($n_0 = 0$). The asymmetry grows with an increase of n_{th} as it was predicted in [14].

In Fig. 2(b) we also compare the results of our computations with the predictions made after the adiabatic elimination of the cavity mode. On one hand the bound for $n_0 = n_{th}$ allowing entanglement predicted by Δ_{EPR} for an electromechanical system [13] ($n_{th} \sim 50$, $\bar{T} \sim 25$ mK) is significantly lower than by logarithmic negativity ($n_{th} > 400$, $\bar{T} > 0.2$ K). On the other hand, if one estimates the logarithmic negativity for the system after adiabatic elimination, this entanglement appears to exist at arbitrary occupations (see dashed black line in Fig. 2(b)). According to the principal considerations in [14] this is possible in blue detuning if the interaction is strong enough which is the case in the pulsed systems.

Robust entanglement with a thermal mechanical oscillator

Andrey A. Rakhubovsky and Radim Filip
rkhbvs@gmail.com

Palacký University Olomouc

Abstract

We consider a protocol to entangle an electromagnetic pulse with a mechanical oscillator at high temperature. We show this protocol to be capable of entangling currently existing experimental systems at relatively high (above the available cryostat) temperatures of the mechanical part. We also predict a possibility of conditional squeezing of the mechanical mode below the shot noise level at the cryostat temperatures.

Proof-of-principle

[R. Filip and V. Kupčík, PRA **87**, 062323 (2013)]

- Two modes (L and M) initially in gaussian states with variances $V_L = 1$ and $V_M \gg 1$.
- Two mode squeezing (AMP) interaction for finite time
- Both modes are attenuated

- There is a threshold g_B for entanglement
- Entanglement is robust against arbitrary attenuation
- There is a higher threshold for conditional squeezing (projecting the noisy mode to a squeezed state by a proper measurement on light) of the noisy mode

Our Approach

We solve quantum Langevin equations for a pulsed system to estimate the covariance matrix

$$\dot{\vec{u}}(t) = \bar{A}\vec{u}(t) + \underbrace{\vec{f}(t)}_{\text{noises}}, \quad \vec{u}(t) = (X_L, P_L, X_M, P_M);$$

$$\vec{u}(t) = \bar{M}(t)\vec{u}(0) + \int_0^t ds\, \bar{M}(t-s)\vec{f}(s); \quad \bar{M}(t) = \exp(\bar{A}t);$$

$$V(t) = \bar{M}(t)V(0)\bar{M}^\top(t) + \int_0^t ds\, ds'\, \bar{M}(t-s)\bar{f}(s,s')\bar{M}^\top(t-s').$$

Knowing the CM we are able to estimate log. negativity and the possibility of conditional squeezing

$$E_N = \max[0, -\ln \nu_-].$$

ν_- is the smaller symplectic eigenvalue of the CM.

Optomechanical coupling

$$H_{int} \propto \underbrace{g_B(a_L^\dagger a_M^\dagger + a_L a_M)}_{\text{AMP}} + \underbrace{g_R(a_L^\dagger a_M + a_L a_M^\dagger)}_{\text{BS}}.$$

The dominant coupling is determined by the detuning $\Delta = \omega_{cav} - \omega_{pump}$, so in the resolved sideband regime ($\Omega_m \ll \kappa$):

- In blue detuning $\omega_{pump} = \omega_{cav} + \Omega_m \Rightarrow$ Two mode squeezing (or amplification), entangles two modes, creates negative mechanical damping.
- In red detuning $\omega_{pump} = \omega_{cav} + \Omega_m \Rightarrow$ Beamsplitter, swaps the quantum states between the modes, creates positive damping.

Pulsed cavity optomechanics

Originally proposed in [Hofer *et al.* PRA **84** (5), 052327] and demonstrated for electromechanics [Palomaki *et al.*, Science **342**, 710 (2013)]

Two pulses enter the cavity sequentially. First, a blue detuned pulse entangles optical and mechanical mode; second, a red detuned one reads the state of mechanical mode.

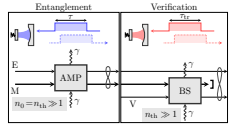

Utilization of pulses relaxes the stability requirement. Input-output relations for entangling protocol

$$A_L^{out} = -\sqrt{\mathrm{T}} A_L^{in} - i\sqrt{1-\mathrm{T}} A_M^{in\dagger}; \quad A_M^{in} = \int_0^\tau a_M^{in}(t) e^{-Gt} dt;$$

$$A_M^{out} = \sqrt{\mathrm{T}} A_M^{in} + i\sqrt{1-\mathrm{T}} A_L^{in\dagger}; \quad A_L^{out} \sim \int_0^\tau a_L^{out}(t) e^{Gt} dt.$$

Which corresponds to AMP interaction with gain $\mathrm{T} = e^{2g_B^2\tau/\kappa} \Rightarrow$ optics and mechanics should be entangled regardless of the temperature of mechanical bath.

Similar input-output relations for red detuning correspond to BS-type interaction between optics and mechanics.

Results

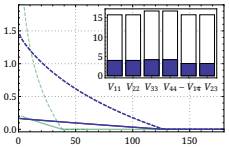

Entanglement between the pulses.

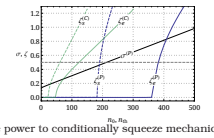

Relative power to conditionally squeeze mechanical mode

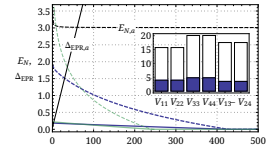

Entanglement between intracavity and mechanical modes.

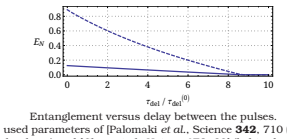

Entanglement versus delay between the pulses.

We used parameters of [Palomaki *et al.*, Science **342**, 710 (2013)] (darker lines) and [Chan *et al.*, Nature **478**, 89] (lighter lines).

bit.ly/upol-posters

What the people typically expect to see on a poster

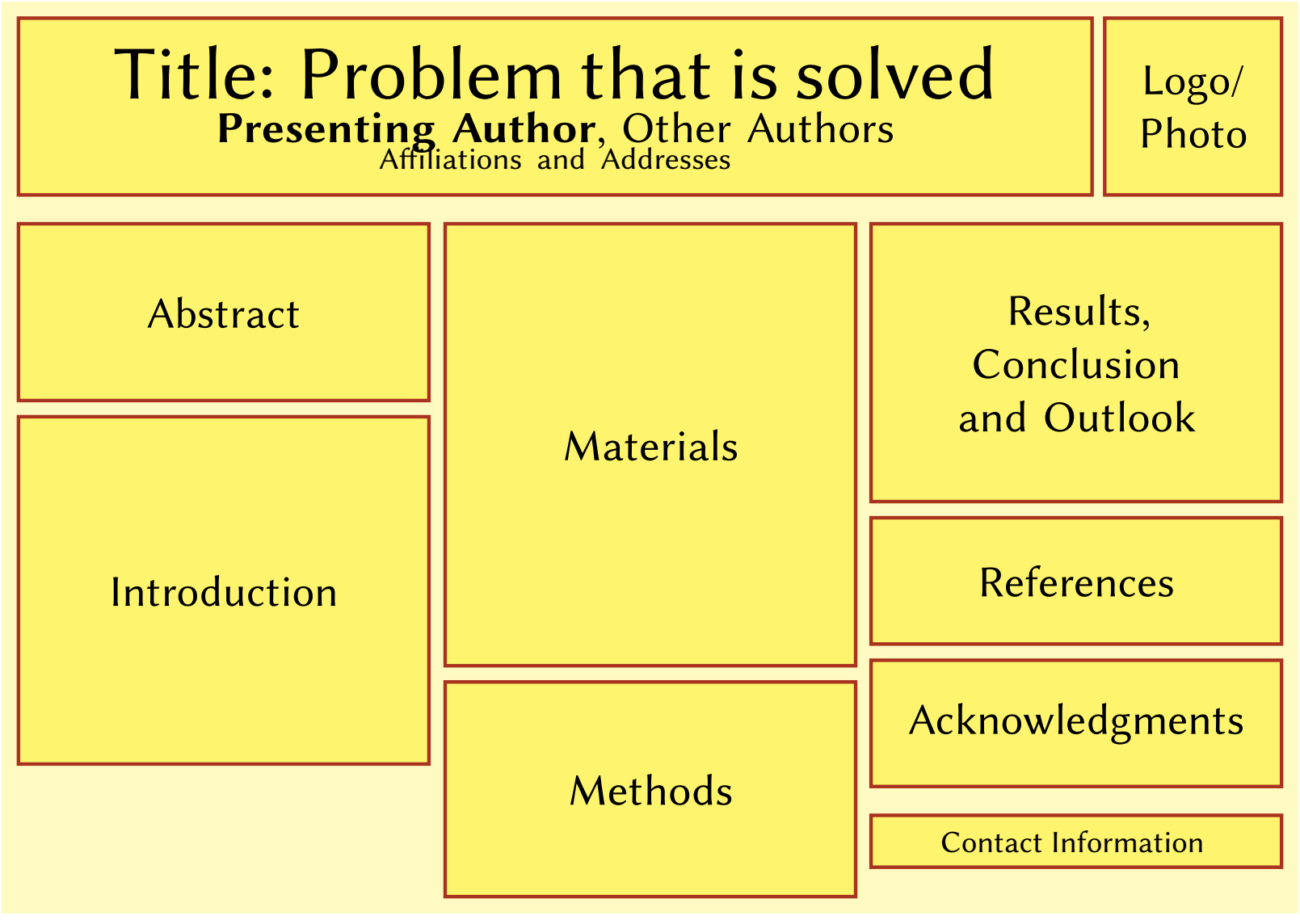

bit.ly/upol-posters

What the people typically expect to see on a poster

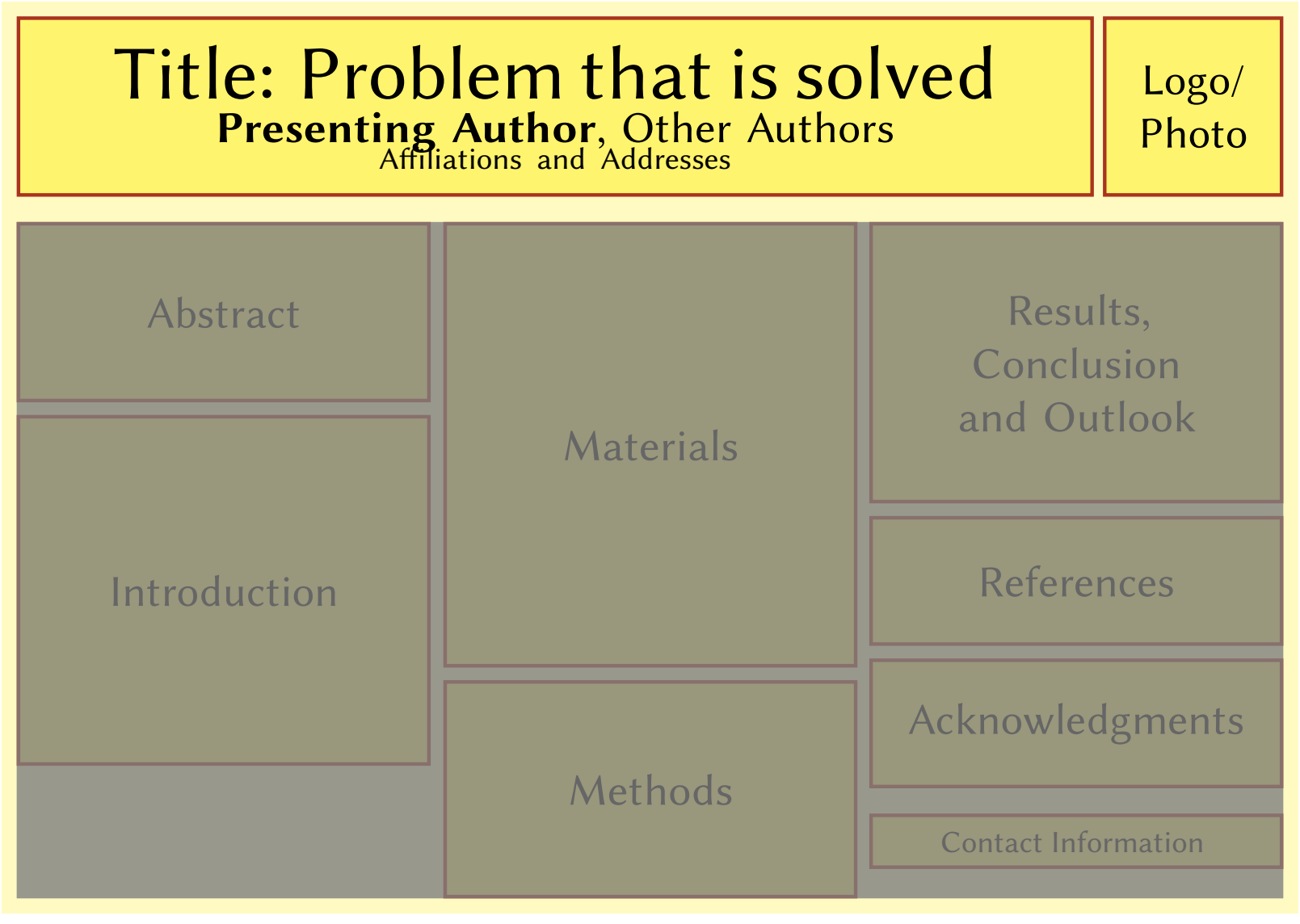

bit.ly/upol-posters

What the people typically expect to see on a poster

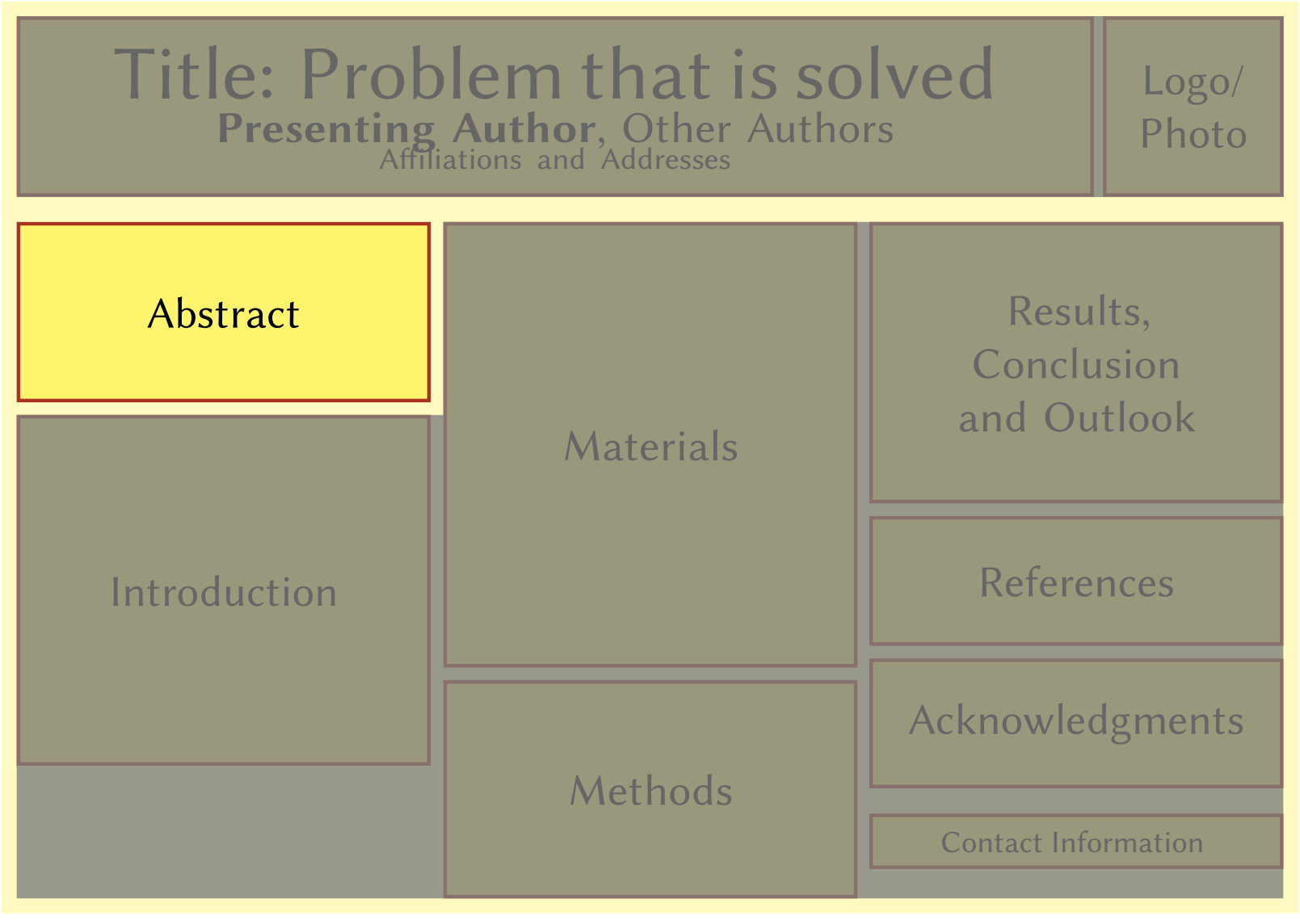

bit.ly/upol-posters

What the people typically expect to see on a poster

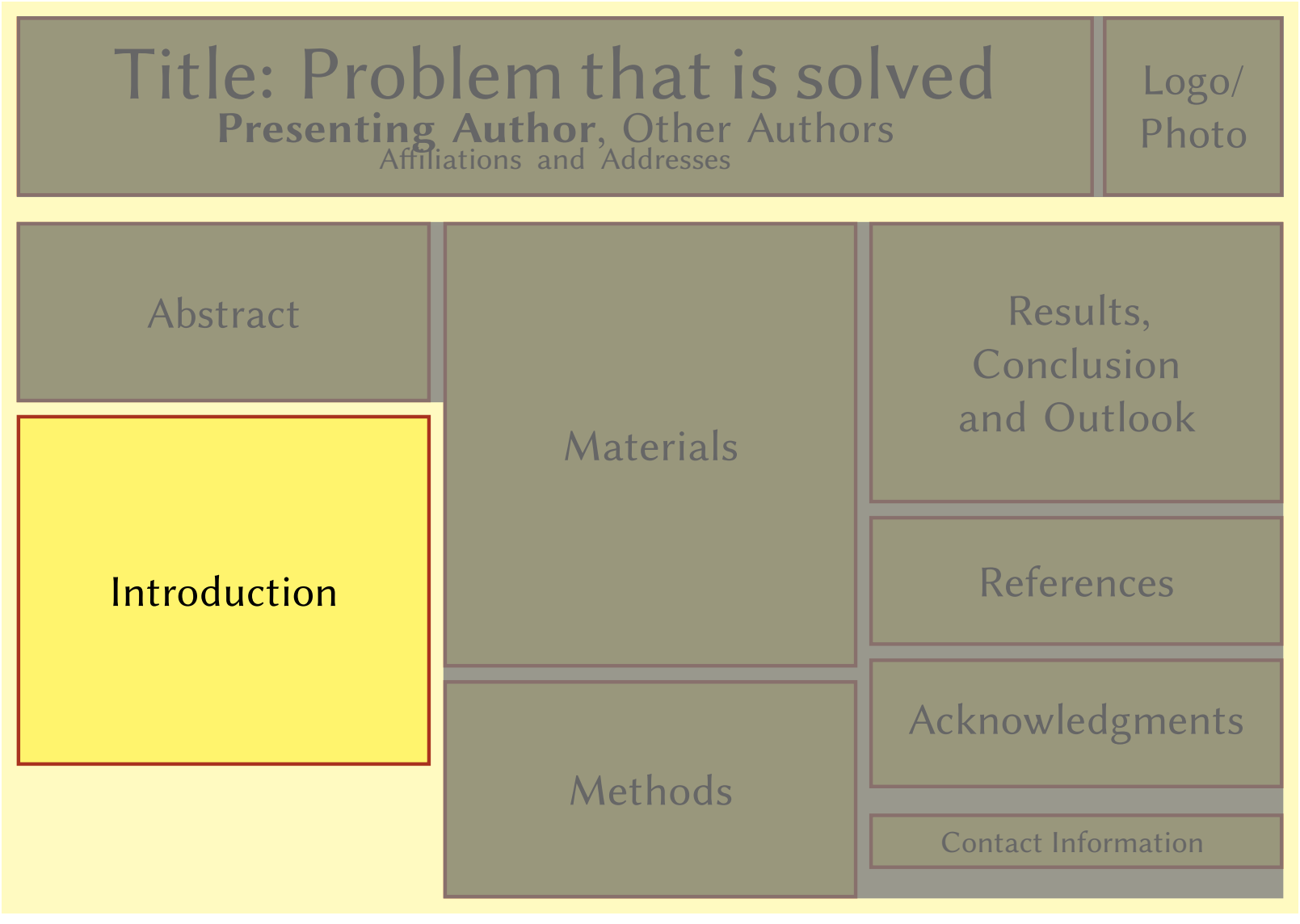

bit.ly/upol-posters

What the people typically expect to see on a poster

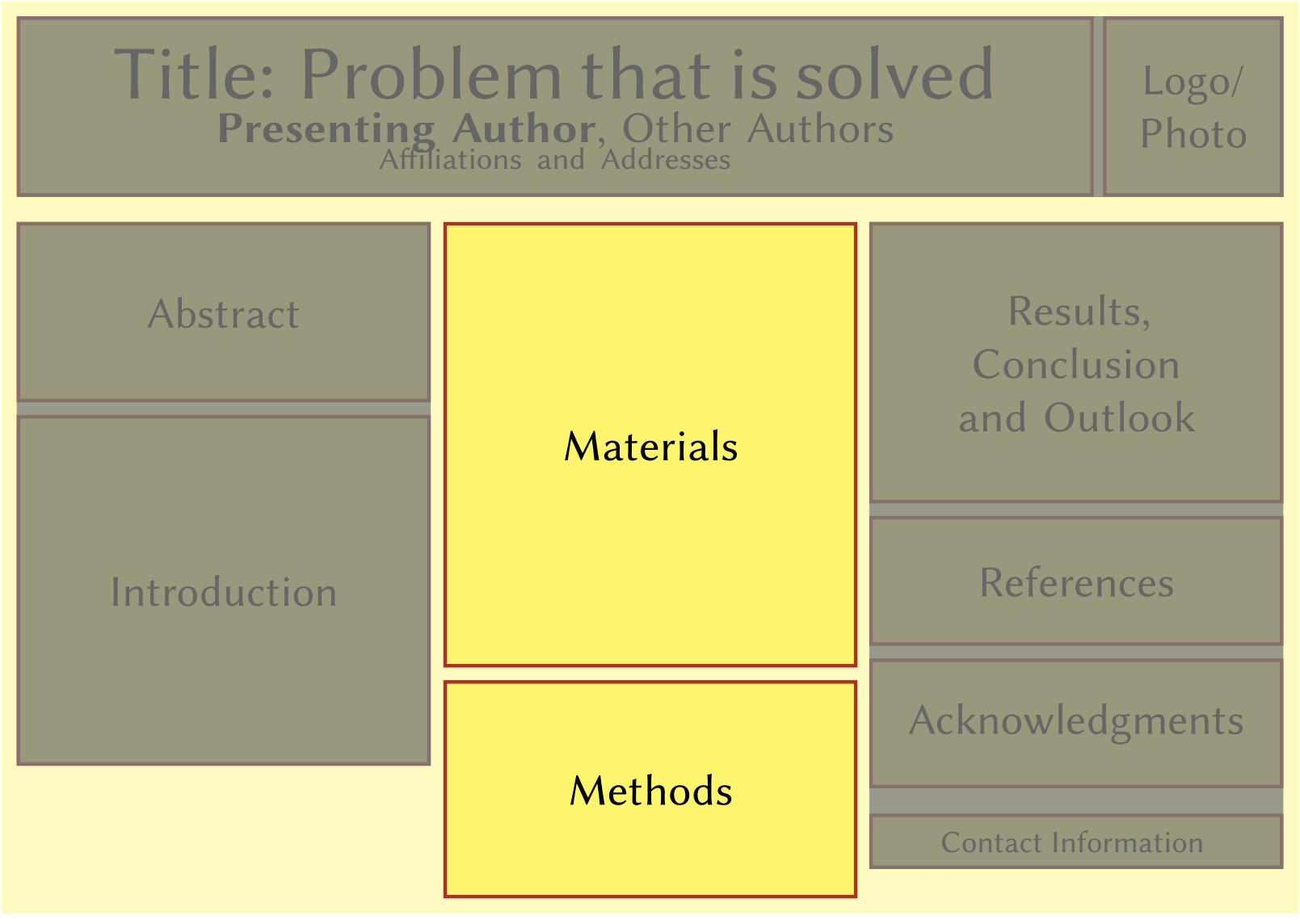

bit.ly/upol-posters

What the people typically expect to see on a poster

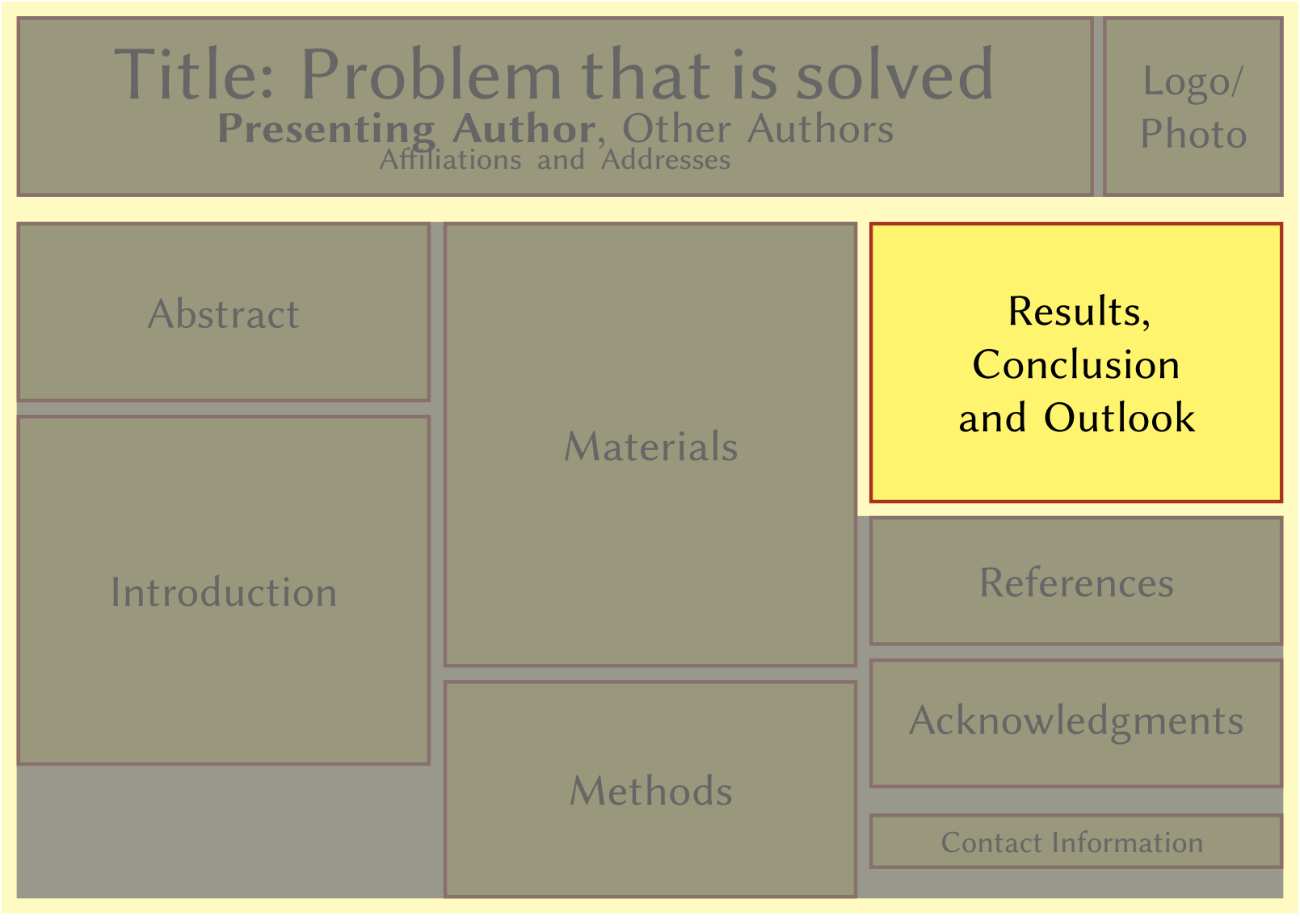

bit.ly/upol-posters

What the people typically expect to see on a poster

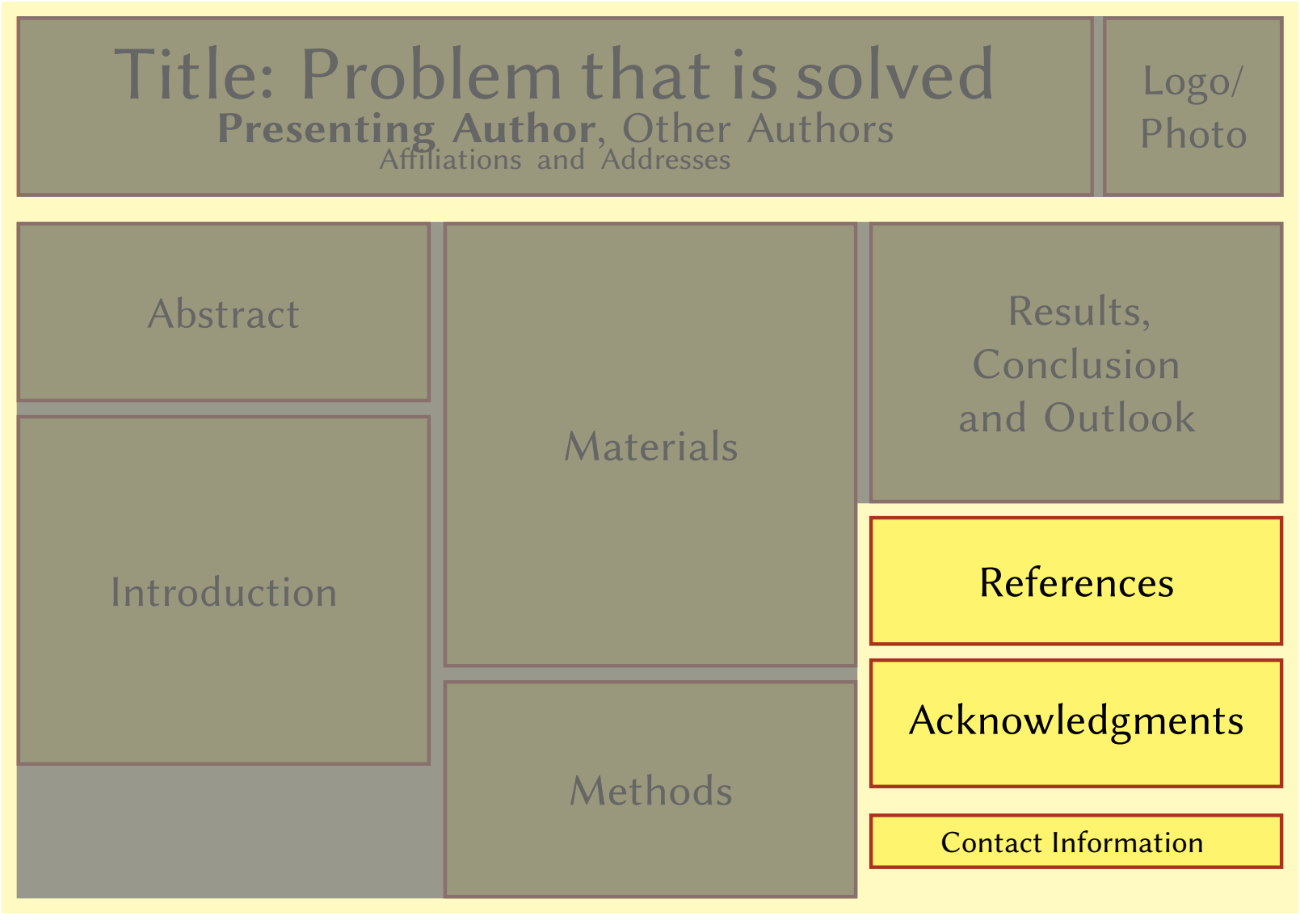

bit.ly/upol-posters

What the people typically expect to see on a poster

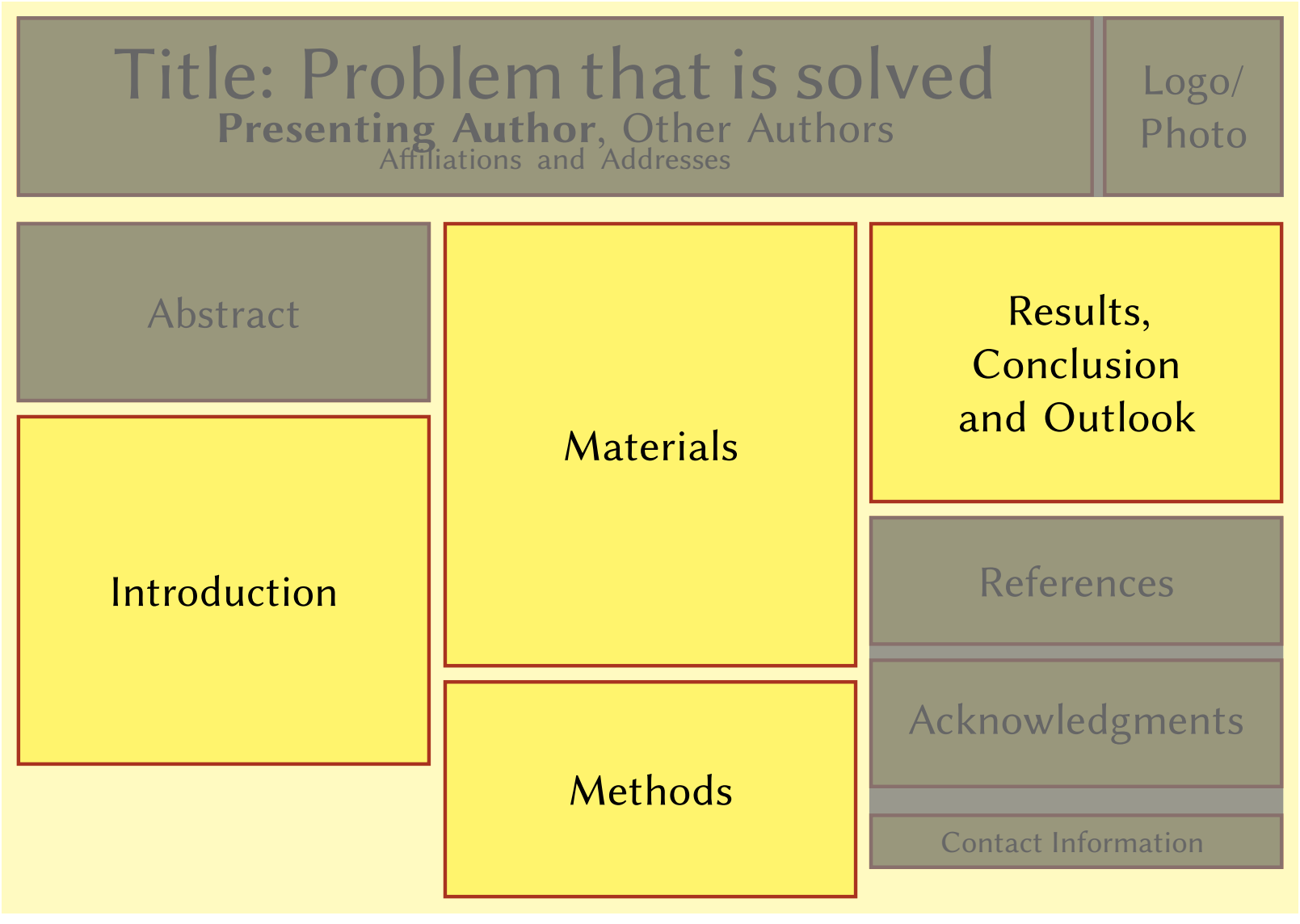

bit.ly/upol-posters

Which is which

Title
Extremely shortened contents

Abstract
Significantly shortened contents

Introduction
Motivation & Reviews & Definitions

Materials&Methods
The contents of your research

Conclusion
Slightly shortened contents

References
List of literature

Contact Information
Your email/ QR codes/ links to articles/ blogs etc.

bit.ly/upol-posters

Outline

Tools (Software)

Presentation making software

- PowerPoint
- OpenOffice/LibreOffice Impress
- Keynote
- Google Slides

Vector Editors

- Adobe Illustrator
- Corel Draw
- Inkscape
- OpenOffice/LibreOffice Draw

Publishing Software

- Microsoft Publisher, Adobe InDesign

LaTeX

- Overleaf template library

bit.ly/upol-posters

Tools (Software)

Presentation making software

PowerPoint
OpenOffice/LibreOffice Impress
Keynote
Google Slides

Vector Editors

Adobe Illustrator
Corel Draw
Inkscape
OpenOffice/LibreOffice Draw

Publishing Software

Microsoft Publisher, Adobe InDesign

LaTeX

Overleaf template library

Web search “Conference Poster Template”

bit.ly/upol-posters

Examples From the Internet

MakeSigns

LOG IN HELP CONTACT US

PRINT MY POSTER RESOURCES ACCESSORIES SHIPPING CART

Here are some PowerPoint templates to get you started. Feel free to change the colors and layout as needed. These templates are within the PowerPoint page size limit of 56" and comes in several different aspect ratios, each of which can be printed in a number of sizes (as listed).

Persuading Sapphire

- 48 x 36 56x42 | 64x48
- 48 x 24 72x36 | 84x42 | 96x48
- 36 x 24 54x36 | 63x42 | 72x48
- 36 x 36 (square) 42x42 | 48x48
- 36 x 48 (vertical) 42x56 | 48x64

Pondering Peacock

- 48 x 36 56x42 | 64x48
- 48 x 24 72x36 | 84x42 | 96x48
- 36 x 24 54x36 | 63x42 | 72x48
- 36 x 36 (square) 42x42 | 48x48
- 36 x 48 (vertical) 42x56 | 48x64

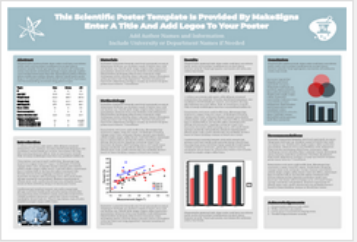

Assessing Slate

- 48 x 36 56x42 | 64x48
- 48 x 24 72x36 | 84x42 | 96x48
- 36 x 24 54x36 | 63x42 | 72x48
- 36 x 36 (square) 42x42 | 48x48
- 36 x 48 (vertical) 42x56 | 48x64

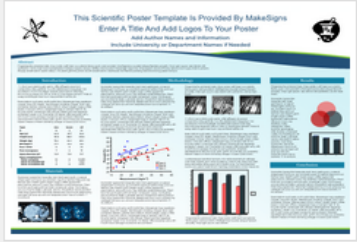

Hypothetical Ocean

- 48 x 36 56x42 | 64x48
- 48 x 24 72x36 | 84x42 | 96x48
- 36 x 24 54x36 | 63x42 | 72x48
- 36 x 36 (square) 42x42 | 48x48
- 36 x 48 (vertical) 42x56 | 48x64

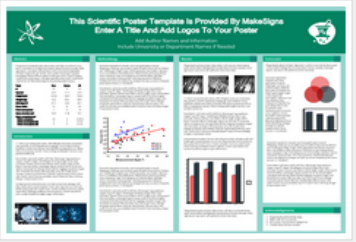

Philosophical Seafoam

- 48 x 36 56x42 | 64x48
- 48 x 24 72x36 | 84x42 | 96x48
- 36 x 24 54x36 | 63x42 | 72x48
- 36 x 36 (square) 42x42 | 48x48
- 36 x 48 (vertical) 42x56 | 48x64

Conceptualizing Cobalt

- 48 x 36 56x42 | 64x48
- 48 x 24 72x36 | 84x42 | 96x48
- 36 x 24 54x36 | 63x42 | 72x48
- 36 x 36 (square) 42x42 | 48x48
- 36 x 48 (vertical) 42x56 | 48x64

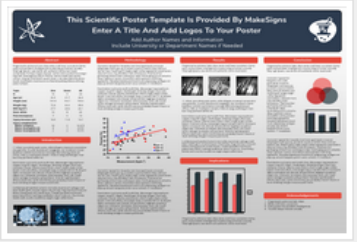

Perceptual Pewter

- 48 x 36 56x42 | 64x48
- 48 x 24 72x36 | 84x42 | 96x48
- 36 x 24 54x36 | 63x42 | 72x48
- 36 x 36 (square) 42x42 | 48x48
- 36 x 48 (vertical) 42x56 | 48x64

Deliberating Watermelon

- 48 x 36 56x42 | 64x48
- 48 x 24 72x36 | 84x42 | 96x48
- 36 x 24 54x36 | 63x42 | 72x48
- 36 x 36 (square) 42x42 | 48x48
- 36 x 48 (vertical) 42x56 | 48x64

Examples From the Internet

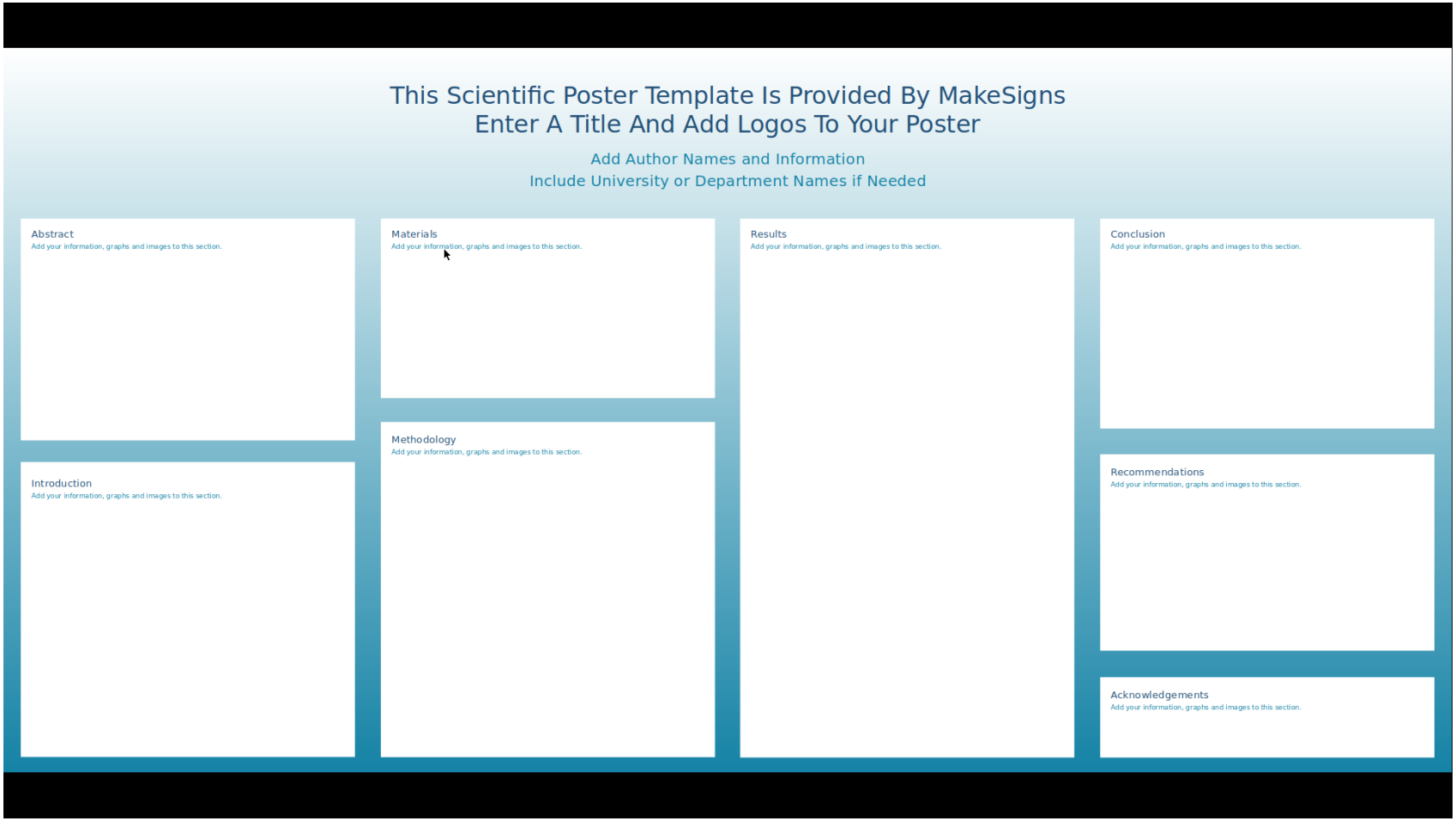

bit.ly/upol-posters

Examples From the Internet

Poster template design: **Aragon**

Standard poster sizes in inches (Height x Width) - Click on a size to download
36x48 | 36x56 | 36x60 | 36x72 | 36x96 | 42x60 | 42x72 | 42x90 | 44x44 | 30x40 | 48x48 | 48x72 | 48x96 | Trifold | Virtual - Standard Screen (4:3 Ratio) | Virtual - Wide Screen (16:9 Ratio)

Standard poster sizes in centimeters (Height x Width) - Click on a size to download
122x91 | 100x70 | 140x100 | 100x100 | 200x100 | A0 | A1

► View Samples ► Learn how to customize the template colors

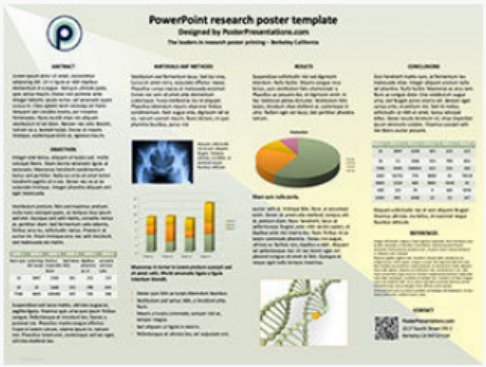

Poster template design: **Beaumont**

Standard poster sizes in inches (Height x Width) - Click on a size to download
36x48 | 36x56 | 36x60 | 36x72 | 36x96 | 42x60 | 42x72 | 42x90 | 44x44 | 30x40 | 48x48 | 48x72 | 48x96 | Trifold | Virtual - Standard Screen (4:3 Ratio) | Virtual - Wide Screen (16:9 Ratio)

Standard poster sizes in centimeters (Height x Width) - Click on a size to download
122x91 | 100x70 | 140x100 | 100x100 | 200x100 | A0 | A1

► View Samples ► Learn how to customize the template colors

Poster template design: **Newfield**

Standard poster sizes in inches (Height x Width) - Click on a size to download
36x48 | 36x56 | 36x60 | 36x72 | 36x96 | 42x60 | 42x72 | 42x90 | 44x44 | 30x40 | 48x48 | 48x72 | 48x96 | Trifold | Virtual - Standard Screen (4:3 Ratio) | Virtual - Wide Screen (16:9 Ratio)

Standard poster sizes in centimeters (Height x Width) - Click on a size to download
122x91 | 100x70 | 140x100 | 100x100 | 200x100 | A0 | A1

► View Samples ► Learn how to customize the template colors

#betterposter on Twitter

Title:
Subtitle

PRESENTER:
Leeroy Jenkins

BACKGROUND: ***Who cares?*** Explain why your study matters in the fastest, most brutal way possible (feel free to add graphics!).

METHODS

1. Collected [what] from [population]
2. Tested it with X process.
3. Illustrate your methods if you can.
4. ***Try a flowchart!***

RESULTS

- Graph/table with ***essential results only***.
- All the other correlations in the ammo bar.

Main finding goes here, translated into **plain English**. **Emphasize** the important words.

Visualize your findings with an image, graphic, or a key figure.

Take a picture to **download** the **full paper**

AMMO BAR

Delete this and replace it with your...

- Extra Graphs
- Extra Correlation tables
- Extra Figures
- Extra nuance that you're worried about leaving out.
- ***Keep it messy!*** This section is just for you.

Leeroy Jenkins, author2, author3, author4, author5, author6, author7, author42

bit.ly/upol-posters

#betterposter on Twitter

How Are You Feeling Today, Dave?

Using IBM's Watson Supercomputer to Extract Emotions from Natural Language

Mike A. Morrison

INTRO

- **IBM Watson** is a supercomputer able to process naturally written language. It can reportedly read a body of text, and extract from that the emotions that the author was feeling when they wrote it.
- **This study** compared Watson's ratings of emotional tone in text to self-report ratings, using a sample of crew members participating in NASA analog science mission in Antarctica.

METHODS

- **Participants:** N = 6 crew members participating in a NASA Science Mission in Antarctica. T = 42 (average) mission days per crew member
- **Diaries:** Crew members **wrote freeform** in **daily diaries** each day . Diaries typically discuss activities from the day, and other crew members.
- **Self-Reports:** Crew members completed self-report measures of psychological distress, happiness, conflict management, and physical activity.
- Using Watson's Alchemy Language service, **Watson analyzed diary text** and reported estimates of Fear, Joy, Sadness, Anger, and Disgust in each diary entry.
- **Analysis:** I tested for significant correlations between Watson's measures of Fear, Joy, Sadness, Anger, and Disgust against a battery of self-report measures of daily attitudes.

RESULTS

- Watson's estimates of happiness and sadness correlate significantly with related self-report measures, but Watson's estimates of disgust, fear, and anger showed no significant correlations.

MICHIGAN STATE UNIVERSITY

IBM Watson can accurately **detect joy** and **sadness** in samples of **written language.**

	Watson **Happiness**	Watson **Sadness**
Self-report **Happiness**	.21**	-.22**
Self-report **Distress**	ns	.19*
Self-report **Conflict Management**	ns	-.24*
Self-report **Physical Activity**	.19**	-.25**

Participants:

- **N = 6** crew members participating in a Science Mission in Antarctica
- **T = 42** (average) mission days per crew member

How do Natural Language Processors Like IBM Watson Work?

1. A software algorithm reads-in a body of text (in this case, a diary entry).
2. The text is converted into features (e.g., frequency of specific words, punctuation usage, sentence length).
3. An algorithm identifies which features in the text are associated with scores on a 'known' criteria (e.g., self-reported happiness, or other-rated emotional tone).
4. Machine learning algorithms create a set of combined language features that reliably predict scores on the criteria of interest in the test data.
5. The 'trained' algorithm looks for these special features in new bodies of text, and outputs an estimate of the criteria.

bit.ly/upol-posters

#betterposter on Twitter

We present a method to accurately and robustly extract inclination angles from red giant stars.

Bayesian hierarchical inference of asteroseismic inclination angles

James S. Kuszlewicz[1,2], William J. Chaplin[2,3], Thomas S.H. North[2,3], Will M. Farr[4,5,6], Keaton J. Bell[1,2], Guy R. Davies[2,3], Tiago L. Campante[7,8], Saskia Hekker[1,2].

Background

The stellar inclination angle is a valuable parameter in many different areas, from characterisation of the geometry of exoplanet and eclipsing binary systems, to stellar populations.

Objective

To accurately and robustly extract inclination angles from red giants.

Methods

1. Select all long-cadence *Kepler* red giants from Stello et al. (2013) where 231μHz < ν_{max} < 270μHz.
2. Identify and fit $\ell = 1$ mixed modes for each star, storing the inclination angle posterior probability density function (PDF) for each mixed mode.
3. Infer inclination angles for each star using a bayesian hierarchical scheme (Hogg et al. 2010) using the individual mode estimates.
4. Test on artificial data to ensure consistency of method.

The model

To model the inclination angle distribution of individual stars we use a modified Fisher distribution. This is characterised by an inclination angle, *i*, a concentration parameter, κ (which scales inversely with the variance), a location parameter, μ (given in radians), and a normalisation constant, φ.

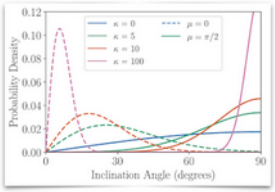

Individual angles and testing with artificial data

An example applied to a single artificial star is shown on the left. The input angle (red dashed line) is close to 50 degrees and the individual PDFs for each mixed mode are plotted in blue. The weighted mean Monte-Carlo estimate is shown in orange and the posterior PDF of the location parameter from the hierarchical analysis is shown in black.

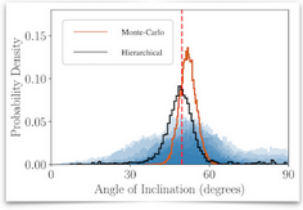

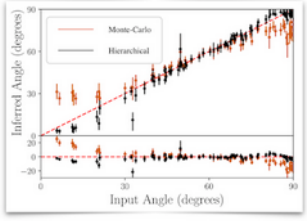

To the left is the inferred inclination angle against the input angle for an artificial sample of stars. The hierarchical method (black) is able to recover the input angle in almost all cases, unlike the Monte-Carlo method (orange) which becomes heavily biased at low and high angles. This can also be seen in the residuals about the 1:1 line (red dashed line) in the bottom panel.

[1]Max-Planck-Institut für Sonnensystemforschung, Göttingen, Germany, email: kuszlewicz@mps.mpg.de
[2]Stellar Astrophysics Centre, Department of Physics and Astronomy, Aarhus University, Denmark
[3]School of Physics and Astronomy, University of Birmingham, Edgbaston, Birmingham, UK
[4]Center for Computational Astrophysics, Flatiron Institute, 162 Fifth Avenue, New York, NY 10010, USA
[5]Department of Physics and Astronomy, Stony Brook University, Stony Brook, NY 11794-3800, USA
[6]School of Physics and Astronomy, Institute of Gravitational Wave Astronomy, University of Birmingham, Edgbaston, Birmingham, UK
[7]Instituto de Astrofísica e Ciências do Espaço, Universidade do Porto, Rua das Estrelas, PT4150-762 Porto, Portugal
[8]Departamento de Física e Astronomia, Faculdade de Ciências da Universidade do Porto, Rua do Campo Alegre, s/n, PT4169-007 Porto, Portugal

Take a picture to download the full paper

References:
Hogg D.W., Myers A.D., Bovy J., 2010, ApJ, 725, 2166
Handberg R., Campante T.L., 2011, A&A, 527, A56
Huber, D., et al., 2012, A&A, 540, A143
Stello D., et al., 2013, ApJ, 765, L41

bit.ly/upol-posters

Use Vector Graphics

Vector

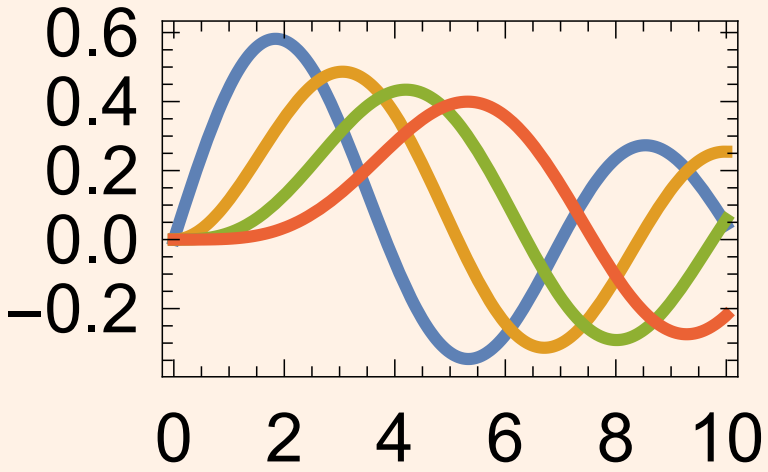

Raster

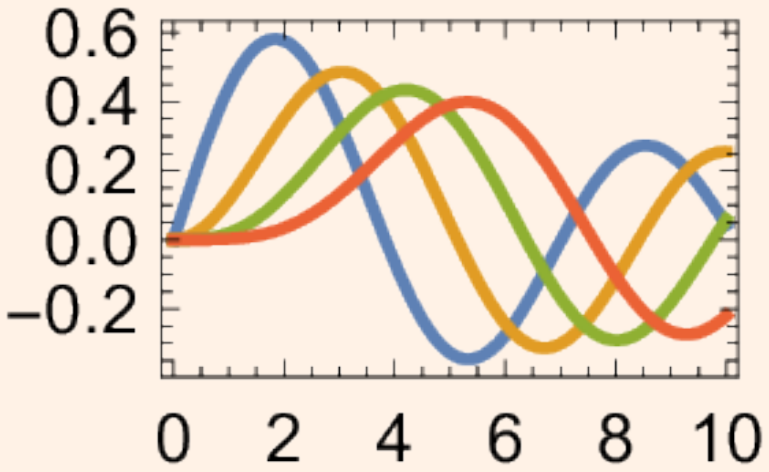

Vector Editors: Adobe Illustrator, Corel Draw, Inkscape, OpenOffice Draw
I use LaTeX which is a markup language

Use Vector Graphics

Vector

Raster

Vector Editors: Adobe Illustrator, Corel Draw, Inkscape, OpenOffice Draw
I use LaTeX which is a markup language

bit.ly/upol-posters

Use Vector Graphics

Vector

Raster

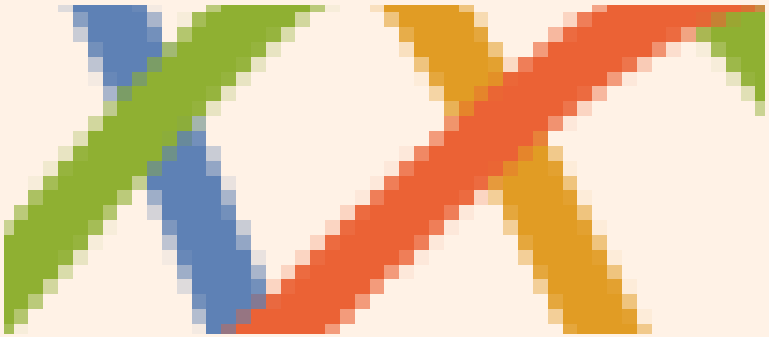

Vector Editors: Adobe Illustrator, Corel Draw, Inkscape, OpenOffice Draw
I use LaTeX which is a markup language

bit.ly/upol-posters

Example Structure

PHYSICAL REVIEW A **91**, 062317 (2015)

Robust entanglement with a thermal mechanical oscillator

Andrey A. Rakhubovsky* and Radim Filip
Department of Optics, Palacký University, 17. listopadu 1192/12, 771 46 Olomouc, Czech Republic
(Received 14 January 2015; published 15 June 2015)

We consider a protocol to entangle an electromagnetic pulse with a mechanical oscillator at high temperature. We show this protocol to be capable of entangling currently existing experimental systems at relatively high (above the available cryostat) temperatures of the mechanical part. We also predict a possibility of conditional squeezing of the mechanical mode below the shot noise level at the cryostat temperatures.

DOI: 10.1103/PhysRevA.91.062317 PACS number(s): 03.67.Bg, 42.50.Wk, 42.50.Ex, 42.50.Dv

I. INTRODUCTION

Quantum optomechanics is a rapidly developing field of quantum physics with continuous variables profiting from the new possibilities of quantum control of mechanical oscillators [1–4]. This hybrid experimental platform directly links the quantum properties of light and microwave radiation, represented by the model of a linear oscillator, with the characteristics of real mechanical-type oscillator. These quantum mechanical oscillators have physical features and capabilities that distinguish them from the properties of light, many times examined in details in continuous-variable quantum optics [5–7]. Mechanical vibration of the real position of the oscillator naturally allows the bridge to thermodynamics and recently ongoing examination of quantum thermodynamics with mechanical oscillators [8–10]. Thinking about this direction at a very basic level, we first admit that the mechanical oscillator is an open system. It naturally tends to thermodynamic equilibrium with its thermal environment. Second, quantum optomechanics can advantageously exploit radiation pressure to push the mechanical oscillators out of thermodynamic equilibrium and, therefore, it allows us to generate interesting quantum effects.

Continuous-variable quantum entanglement [5] is a basic phenomenon demonstrating the connection between light and mechanical oscillator out of thermal equilibrium. Theoretically, an interaction caused by radiation pressure allows the entangling process of amplification of mechanical vibration and radiation at the same time [2]. In quantum optics, such amplification processes in nonlinear crystals lead to the generation of squeezed states of light and Gaussian entanglement between optical beams [7]. These are useful resources for a variety of operations developed in quantum optics and quantum information processing [7,11,12]. In quantum optics, it is easy to achieve the ground state of the mode of light modeled by the linear harmonic oscillator since the light interacts very weakly with matter and the modes can be easily blocked. On the other hand, the mechanical oscillators are inherently thermally occupied by phonons and their cooling is necessary by use of sophisticated techniques [4]. For the intensively cooled electromechanical oscillators, Gaussian quantum entanglement has been recently experimentally demonstrated in the pulsed regime [13]. At the same time, it was theoretically predicted that Gaussian quantum entanglement is observable at the output of the amplification process for thermal-equilibrium input states with arbitrary temperature [14]. These methods could, in principle, generate *thermal* entanglement without any cooling mechanical oscillators and also the mechanical squeezed state of the mechanical oscillator. Such thermal entanglement does not naturally occur in optical nonlinear processes, so this type of thermal Gaussian entanglement has not been studied in quantum optics. In pulsed quantum optomechanics it is possible to achieve an ideal amplification regime approximatively by an adiabatic elimination of the optical mode when the mechanical oscillator is not much thermally occupied [15–17]. Unfortunately, this approximation is generally not applicable for an interesting case of extreme temperature of the mechanical oscillator, where thermal entanglement can still be surprisingly detected.

In this paper, the pulsed generation of thermal entanglement between light and mechanical oscillator is analyzed without using the adiabatic approximation. The bound on generation of the entanglement is defined in the limit of the large temperature of the mechanical oscillator. Generation of thermal entanglement is analyzed for the current electromechanical experiment [13] and subsequently for the future optomechanical experiment [18]. For both types of experiments, existence and robustness of the thermal Gaussian entanglement is confirmed for the large number $n_{th} \approx 400$ of thermal phonons for the experiment in [13] and $n_{th} \approx 240$ for the experiment in [18]. In addition, it is shown that thermal entanglement allows

*andrey.rakhubovsky@upol.cz

FIG. 1. (Color online) Protocol to create and verify entanglement. First the bias-detuned entangling pulse with length τ enters the cavity, then after the delay time τ_{del} the red-detuned pulse lasting τ_0 performs the read-out of the state of the mechanical subsystem. Mechanical system is initially in a thermal state with occupation n_{th} and is coupled at the rate γ to the thermal bath with occupation n_{th}.

TABLE I. Values of parameters used for numerical estimations.

Quantity	Palomaki *et al.* [13]	Chan *et al.* [18]
Mechanical frequency ω	$2\pi \times 10.34$ MHz	$2\pi \times 3.9$ GHz
Viscous damping rate γ	$2\pi \times 35$ Hz	$2\pi \times 39$ kHz
Cavity half width κ	$2\pi \times 180$ kHz	$2\pi \times 0.25$ GHz
Sideband resolution parameter κ/ω	0.02	0.06
Single-photon coupling g_0	$2\pi \times 200$ Hz	$2\pi \times 0.9$ MHz
Photon number $n_{cav} = n_{cav}$	26×10^3	1.5×10^3
Enhanced coupling $g_R = g_B$	$2\pi \times 30.9$ kHz	$2\pi \times 35.0$ MHz
Coupling $G_R = G_B =: G_0$	$2\pi \times 5.3$ kHz	$2\pi \times 9.8$ MHz
Duration of entangling pulse τ	35 μs	0.13 μs
Time span between the pulses $\tau_{del}^{(0)}$	10 μs	0.04 μs
Duration of the verification pulse τ_0	30 τ	30 τ

to underestimation of entanglement in case the state being analyzed is asymmetric (i.e., variances of one of the modes are exceedingly higher than those of the another). According to the recent research [14] this is the very case of the optomechanical entanglement particularly at higher temperatures. To avoid this we use logarithmic negativity [20] as a measure of entanglement. For a brief review of the mentioned measures of entanglement we refer the reader to Appendix A.

Our analysis complements the results previously reported owing to several differences. First we carry out a complete numerical analysis of the system described by Eq. (1) with the only approximation of rotating wave (which is justified by good sideband resolution $\kappa/\omega \ll 1$ in the setups we consider; see Table I). In our calculations we do not use the adiabatic elimination of the cavity mode. Second, as a criterion for the presence of the mechanical we use logarithmic negativity [20] instead of EPR variance [28]. Applying this distinctive feature we analyze to which extent the recent predictions of robust entanglement [14,17] in optomechanical systems are valid.

In the experiment [13] the pulsed protocol was realized in an electromechanical setup. The mechanical mode was pre-cooled using an additional red detuned pulse. The entanglement between the mechanics and field was then quantified by measuring the covariance matrix of quadratures of pulses leaking from the circuit. Below in comparison to the results of [13,15] we present analysis of the entanglement between these two pulses as well as the analysis of the entanglement between the mechanical mode and the entangling pulse.

IV. ESTIMATION OF COVARIANCE MATRIX

The linearized equations of motion for the system read in matrix form,

$$\dot{u}(\tau) = Au(\tau) + f(\tau),$$

where $u = (X, Y, q, p)$ is the vector of intracavity quadratures and $f = (\sqrt{2\kappa}X^{in}, \sqrt{2\kappa}Y^{in}, \sqrt{2\Gamma}q_{in}, \sqrt{2\Gamma}p_{in})$ is the vector of Langevin forces; X, Y and X^{in}, Y^{in} are the quadratures, respectively, of the intracavity field a and the Langevin force a^{in}. The form of the so-called drift matrix A peculiar to a particular type of interaction can be deduced from the general form [13,28],

$$A = \begin{pmatrix} -\kappa & 0 & g_R & g_B \\ 0 & -\kappa & -g_B & -g_R \\ g_R & g_B & -\gamma/2 & 0 \\ -g_B & -g_R & 0 & -\gamma/2 \end{pmatrix}$$

by equating $g_R = 0$ for the blue detuned pulse, $g_B = 0$ for the red detuned pulse or both $g_R = g_B = 0$ for the free evolution between the pulses ($g_{R,B}$ denote the optomechanical coupling enhanced by a number of intracavity photons in the corresponding pulse; $g_{\circ} \equiv g_0\sqrt{n_{cav}}$, $k = B, R$).

The system under consideration is initially in a Gaussian state and the linear dynamics preserves this quality. So the correlation properties of the system can be completely characterized by its two first moments, of which we are interested in second ones, namely the covariance matrix (CM) with elements defined as

$$V_{ij}(\tau) := \langle u_i(\tau) \circ u_j(\tau) \rangle. \tag{4}$$

To estimate it we use the approach similar to the one of Refs. [30,31]. The solution of the equations of motion could be formally written in the form,

$$u(\tau) = M(\tau - t_0)u(t_0) + \int_{t_0}^{\tau} ds M(\tau - s) f(s), \tag{5}$$

where M is the matrix exponential $M(t) = \exp(At)$. Performing substitution of the equation above into the definition of elements of the CM and integrating the order of integration and averaging one can obtain the expression for the covariance matrix of the intracavity quadratures:

$$V(t) = M(t - t_0)V(t_0)M^{\top}(t - t_0) + \int_{t_0}^{t} ds M(t - s)F M^{\top}(t - s),$$

where $^{\top}$ stands for transposition, F is a matrix of correlations between the Langevin forces:

$$\langle f_i(s) \circ f_j(s') \rangle \equiv F\delta(s - s') = \mathrm{diag}\left[\kappa, \kappa, \gamma\left(n_{th} + \tfrac{1}{2}\right), \gamma\left(n_{th} + \tfrac{1}{2}\right)\right]\delta(s - s').$$

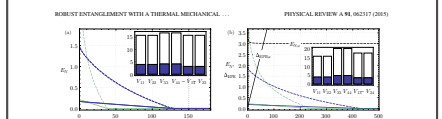

FIG. 2. (Color online) Different types of entanglement (logarithmic negativity) versus the temperature (occupation number) of the mechanical subsystem. (a) Entanglement between the quadratures of the entangling and the verification pulses. (b) Entanglement between the entangling pulse and the mechanical mode. Darker (blue) traces, electromechanical experimental setup reported by Palomaki *et al.* [13]; lighter (green) traces, optomechanical crystal by Chan *et al.* [18]. Dashed lines, lossless case; solid lines, realistic damping in both modes, $\eta = 0.2$. (Inset) Nonzero elements of covariance matrix simulating the experiment from Ref. [13] (initial mechanical occupation $n_0 = 0$, mechanical bath occupation $n_{th} = 40$). Black lines in (b) represent logarithmic negativity $E_{N,a}$ and EPR variance $\Delta_{EPR,a}$ of the optomechanical system calculated after the adiabatic elimination of the cavity mode. For the parameters utilized for estimations see Table I.

In [13] the entanglement was authenticated by analysis of the covariance matrix between the quadratures of the entangling pulse and the verification pulse. These quantities following the considerations of [15] were defined by projection of the leaking field quadratures $u^{out} = (X^{out}, Y^{out})$ on the exponential envelopes. Explicitly this projection reads

$$U^{\pm} = C_{\pm}\int_{\tau_{del}} dx e^{\mp\frac{\gamma}{2}x} u^{out}, \quad U^{\pm} = C_{\pm}\int_{\tau_{del}}^{\tau} dx e^{\mp\frac{\gamma}{2}x} u^{out}. \tag{6}$$

The integration is done over the duration of corresponding pulse denoted as $T_{R,B}$; $C_{\pm,R}$ is the normalizing coefficient, so $\langle U_i^{\pm} U_i^{\pm}\rangle = 1$, where $k = B, R$. The exponential rates are defined as $\tilde{G}_k := g_k^2/\kappa$.

The quadratures of the leaking field are computed using the usual input-output relations [32],

$$u_j^{out}(x) = \sqrt{2\kappa}\, u_j(t) - u_j^{in}(t), \quad j = 1,2. \tag{7}$$

Here $u^{in} = (X^{in}, Y^{in})$ denotes the vector of quadratures of the input field. Please note that both u^{out} and u^{in} are two-dimensional vectors so only the first two components of u are used.

Using the definitions given one can make estimations for the covariance matrix of the quadratures of the two pulses. The matrix is written as follows with the help of 2×2 blocks that contain autocorrelations of and cross correlations between the two pulses,

$$\mathbb{V}_{ij} = \begin{pmatrix} \langle U_i^{B,R} \circ U_j^{B,R}\rangle & \langle U_i^{B,R} \circ U_j^{T,V}\rangle \\ \langle U_i^{T,V} \circ U_j^{B,R}\rangle & \langle U_i^{T,V} \circ U_j^{T,V}\rangle \end{pmatrix}, \quad i,j = 1,2.$$

To compute the elements of $\mathbb{V}_{ij}$ we use the same approach. We substitute the formal solution (5) and the definition of pulse quadratures (6) into the input-output relations (7). After swapping the order of the averaging over state and of the integration over time we are able to relate $\mathbb{V}_{ij}$ with the covariance matrix V_0 of the initial state of the system and the correlations of the Langevin forces. In more details, for instance, for $\langle U_i^B \circ U_j^R\rangle$ one can obtain

$$\langle U_i^B \circ U_j^R\rangle = C_B^2 \int_0^{\tau}\int_0^{\tau} ds\, ds' e^{\frac{\gamma}{2}(s+s')} \times 2\kappa\Big[M(s)V_0 M^{\top}(s') + \int_0^{s} du\, ds' M(s-u)F\delta(u-s')M^{\top}(s'-s') - \int_0^{s} du M(s-u)\tilde{F}(u-s') - \int_0^{s'} ds' \tilde{F}(s'-s)M^{\top}(s'-s') + \frac{1}{2\kappa}\tilde{F}(0-s')\Big]_{ij}, \quad i,j = 1,2.$$

In this equation we introduced a new matrix $\tilde{F}$ characterizing correlations between the intracavity Langevin forces (elements of f) and the quadratures of incident field a^{in}, namely,

$$\langle \tilde{F}(s-s')_{ij} = \langle u_i^{in}(s) \circ u_j^{in}(s')\rangle = \mathrm{diag}\left[\tfrac{1}{2}, \tfrac{1}{2}, 0, 0\right]\delta(s-s').$$

The mechanical subsystem is assumed to be initially in a thermal state with occupation number n_{th} and each mode the cavity is assumed to be in vacuum, so the covariance matrix of the initial state is as follows:

$$V_0 = \mathrm{diag}\left[\tfrac{1}{2}, \tfrac{1}{2}, n_0 + \tfrac{1}{2}, n_0 + \tfrac{1}{2}\right].$$

V. RESULTS OF COMPUTATION

A. Verification of entanglement

To prove the validity of our method we first compare the results we obtain with the experimental ones reported in Ref. [13], namely we estimate the covariance matrix of the two consequent pulses (the entangling and verification ones) for the same experimental setup.

The result of numerical analysis is presented in Fig. 2(a) (for the exact values of parameters we used for estimations please see Table I). There is the figure representation of the elements of the covariance matrix of the quadratures of two pulses for a pre-cooled close to the ground-state mechanical oscillator in a cryogenic bath ($n_0 = 0$, $n_{th} = 40$). Empty bars correspond to the elements obtained in the case of perfect detection ($\eta = 1$) and solid bars correspond to attenuation in both modes $\eta = 0.2$. We see here a good quantitative coincidence with the reported experimental results.

The figure contains two pairs of traces of logarithmic negativity between the two pulses versus the mechanical occupation. The initial occupation n_0 of the mechanical mode along the traces is assumed to be equal to the occupation n_{th} of the mechanical bath (the mechanical mode is assumed to be at equilibrium state with its environment).

The darker curves employ the parameters reported in Ref. [13]. The logarithmic negativity is computed under the assumption of perfect detectors and absence of losses (dashed line) and under the realistic assumption of damping in both modes with effective transmittance $\eta = 0.2$ (solid line) due to nonperfect detection.

It is clear from the figure that the entanglement between the pulses is robust against temperature of the mechanical environment which proves the pre-cooling stage is unnecessary in the entangling protocol (the maximum temperature allowing entanglement is $\sim$65 mK, about three times higher than the temperature of the cryostat). Comparison of the traces demonstrates that the damping in both modes does not completely destroy the entanglement but only decreases its value, i.e., the entanglement is robust against attenuation in both modes. It is a clear witness that the robust version of thermal entanglement predicted in [14] can be observed in recent experiment [13].

The two steeper (lighter) curves in Fig. 2(a) represent logarithmic negativity computed for the same protocol within the entangling-cryostat experimental setup reported in Ref. [18]. Although the phonon number boundary is lower in this case, one should note that the frequency of the mechanical mode is several orders higher in this experiment and owing to this the boundary temperature is actually higher (more than 40 K, twice as high as the temperature of the corresponding cryostat, 20 K).

It needs to be underlined that the negativity estimated in Fig. 2(a) is the measure of entanglement between the two *pulses* emerging from the cavity but not between field and matter although the entanglement is created by means of optomechanical interaction.

It is also illustrative to check how the entanglement between the pulses can tolerate longer separations between the pulses. The dependence of the logarithmic negativity on the time separation of the pulses (in units of $\tau_{del}^{(0)}$ used to plot Fig. 2) is presented in Fig. 3. It shows, for instance, that the entanglement between the two pulses can persist even when the time span between them is twice as long as the duration of the entangling pulse.

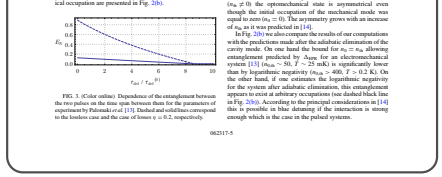

FIG. 3. (Color online) Dependence of the entanglement between the two pulses on the time span between them for the parameters of experiment by Palomaki *et al.* [13]. Dashed and solid lines correspond to the lossless case and the case of losses $\eta = 0.2$, respectively.

B. Optomechanical entanglement

Another figure of merit is the optomechanical entanglement between the motion of the mechanical subsystem and the quadratures of the leaking field immediately after the entangling pulse. This entanglement exhibits even stronger robustness against the noisy thermal bath of the mechanical mode. The traces of logarithmic negativity versus the mechanical occupation are presented in Fig. 2(b).

The two pairs of lighter curves represent the logarithmic negativity estimated using our approach versus the mechanical occupation for Refs. [13] and [18]. The optomechanical entanglement in this setup appears to be robust to both the temperature of the mechanical bath and the initial temperature of mechanical mode as well as robust to attenuation in both mechanical and optical modes.

In the inset to Fig. 2(b) one can see the visualization of nonzero elements of the covariance matrix between the blue pulse and the mechanical mode after the (entangling) interaction is complete. Comparison of the covariance matrix with one of the two pulses reveals that the verification (red detuned) pulse does indeed perform state transfer from the mechanical mode to the leaking field with efficiency close to the ratio κ_{ext}/κ of two decay rates: the one due to the coupling of the circuit to the transmission line and the total decay rate of the circuit. The residual discrepancy is caused by the mechanical decoherence taking place during the interval between the pulses.

Due to the nonzero temperature of the mechanical bath ($n_{th} \neq 0$) the optomechanical state is asymmetrical even though the initial occupation of the mechanical mode was equal to zero ($n_0 = 0$). The asymmetry grows with an increase of n_{th} as it was predicted in [14].

In Fig. 2(b) we also compare the results of our computations with the predictions made after the adiabatic elimination of the cavity mode. On one hand the bound for $n_0 = n_{th}$ allowing entanglement predicted by Δ_{EPR} for an electromechanical system [13] ($n_{th} \sim 50$, $\bar{T} \sim 25$ mK) is significantly lower than by logarithmic negativity ($n_{th} > 400$, $\bar{T} > 0.2$ K). On the other hand, if one estimates the logarithmic negativity for the system after adiabatic elimination, this entanglement appears to exist at arbitrary occupations (see dashed black line in Fig. 2(b)). According to the principal considerations in [14] this is possible in blue detuning if the interaction is strong enough which is the case in the pulsed systems.

Robust entanglement with a thermal mechanical oscillator

Andrey A. Rakhubovsky and Radim Filip
rkhbvs@gmail.com

Palacký University Olomouc

Abstract

We consider a protocol to entangle an electromagnetic pulse with a mechanical oscillator at high temperature. We show this protocol to be capable of entangling currently existing experimental systems at relatively high (above the available cryostat) temperatures of the mechanical part. We also predict a possibility of conditional squeezing of the mechanical mode below the shot noise level at the cryostat temperatures.

Proof-of-principle

[R. Filip and V. Kupčík, PRA **87**, 062323 (2013)]

- Two modes (L and M) initially in gaussian states with variances $V_L = 1$ and $V_M \gg 1$.
- Two mode squeezing (AMP) interaction for finite time
- Both modes are attenuated

- There is a threshold g_B for entanglement
- Entanglement is robust against arbitrary attenuation
- There is a higher threshold for conditional squeezing (projecting the noisy mode to a squeezed state by a proper measurement on light) of the noisy mode

Our Approach

We solve quantum Langevin equations for a pulsed system to estimate the covariance matrix

$$\dot{\tilde{u}}(t) = \tilde{A}\tilde{u}(t) + \underbrace{\tilde{f}(t)}_{\text{noises}}, \quad \tilde{u}(t) = (X_L, P_L, X_M, P_M);$$

$$\tilde{u}(t) = \tilde{M}(t)\tilde{u}(0) + \int_0^t ds\, \tilde{M}(t-s)\tilde{f}(s); \quad \tilde{M}(t) = \exp(\tilde{A}t);$$

$$V(t) = \tilde{M}(t)V(0)\tilde{M}^{\top}(t) + \int_0^t ds\, ds'\, \tilde{M}(t-s)\tilde{f}(s,s')\tilde{M}^{\top}(t-s').$$

Knowing the CM we are able to estimate log. negativity and the possibility of conditional squeezing

$$E_N = \max[0, -\ln \nu_-].$$

ν_- is the smaller symplectic eigenvalue of the CM.

Optomechanical coupling

$$H_{int} \propto \underbrace{g_B(a_L^{\dagger}a_M^{\dagger} + a_L a_M)}_{\text{AMP}} + \underbrace{g_R(a_L^{\dagger}a_M + a_L a_M^{\dagger})}_{\text{BS}}.$$

The dominant coupling is determined by the detuning $\Delta = \omega_{cav} - \omega_{pump}$, so in the resolved sideband regime ($\Omega_m \ll \kappa$):

- In blue detuning $\omega_{pump} = \omega_{cav} + \Omega_m \Rightarrow$ Two mode squeezing (or amplification), entangles two modes, creates negative mechanical damping.
- In red detuning $\omega_{pump} = \omega_{cav} + \Omega_m \Rightarrow$ Beamsplitter, swaps the quantum states between the modes, creates positive damping.

Pulsed cavity optomechanics

Originally proposed in [Hofer *et al.* PRA **84** (5), 052327] and demonstrated for electromechanics [Palomaki *et al.*, Science **342**, 710 (2013)]

Two pulses enter the cavity sequentially. First, a blue detuned pulse entangles optical and mechanical mode; second, a red detuned one reads the state of mechanical mode.

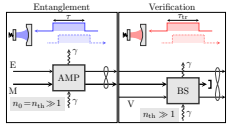

Utilization of pulses relaxes the stability requirement. Input-output relations for entangling protocol

$$A_L^{out} = -\sqrt{\Gamma}A_L^{in} - i\sqrt{1-\Gamma}A_M^{in\dagger}; \quad A_L^{in} = \int_0^{\tau} a_L^{in}(t)e^{-Gt}dt;$$

$$A_M^{out} = \sqrt{\Gamma}A_M^{in} + i\sqrt{1-\Gamma}A_L^{in\dagger}; \quad A_L^{out} \sim \int_0^{\tau} a_L^{out}(t)e^{Gt}dt.$$

Which corresponds to AMP interaction with gain $\Gamma = e^{2g_B^2\tau/\kappa} \Rightarrow$ optics and mechanics should be entangled regardless of the temperature of mechanical bath.

Similar input-output relations for red detuning correspond to BS-type interaction between optics and mechanics.

Results

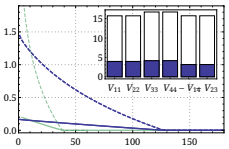

Entanglement between the pulses.

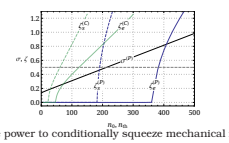

Relative power to conditionally squeeze mechanical mode

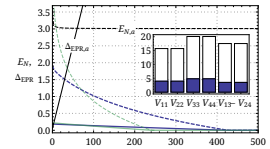

Entanglement between intracavity and mechanical modes.

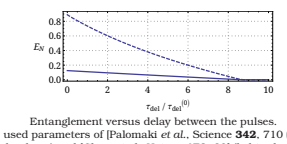

Entanglement versus delay between the pulses.

We used parameters of [Palomaki *et al.*, Science **342**, 710 (2013)] (darker lines) and [Chan *et al.*, Nature **478**, 89] (lighter lines).

bit.ly/upol-posters

Importance of Vector graphics

Importance of Vector graphics

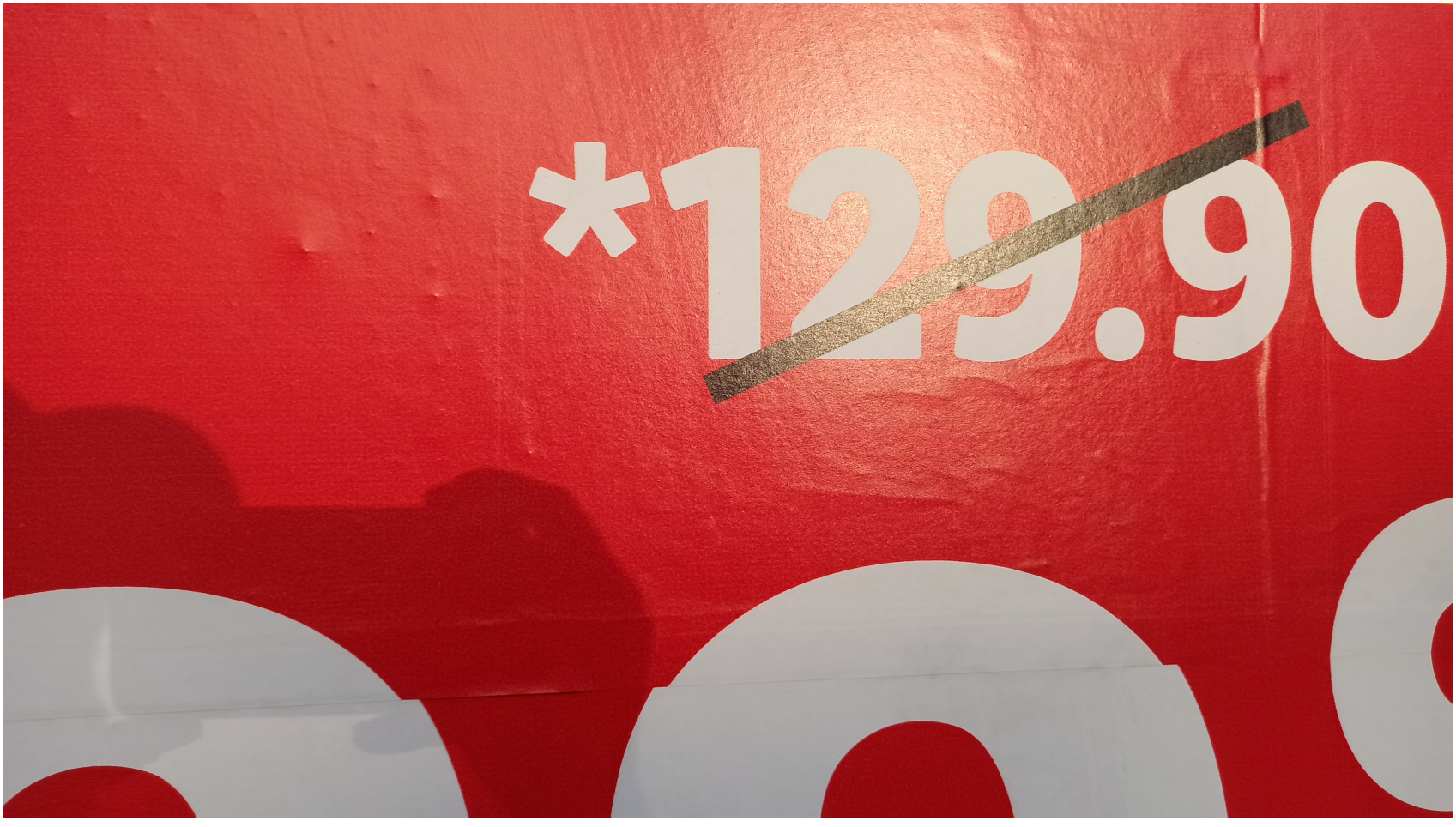

Importance of Vector graphics

bit.ly/upol-posters

Which Fonts to Use

Sans-Serif

It doesn't matter how beautiful your theory is, it doesn't matter how smart you are. If it doesn't agree with experiment, it's wrong.

Richard Feynman

Serif

It doesn't matter how beautiful your theory is, it doesn't matter how smart you are. If it doesn't agree with experiment, it's wrong.

Richard Feynman

Sans-Serif fonts: Helvetica, Arial, Bitstream Vera, DejaVu, whatever
I use Linux Biolinum / Linux Libertine
Avoid Microsoft ComicSans

Font Size

Use Large Font!

Text	24 pt
Headings	48 pt
Titles	72 pt

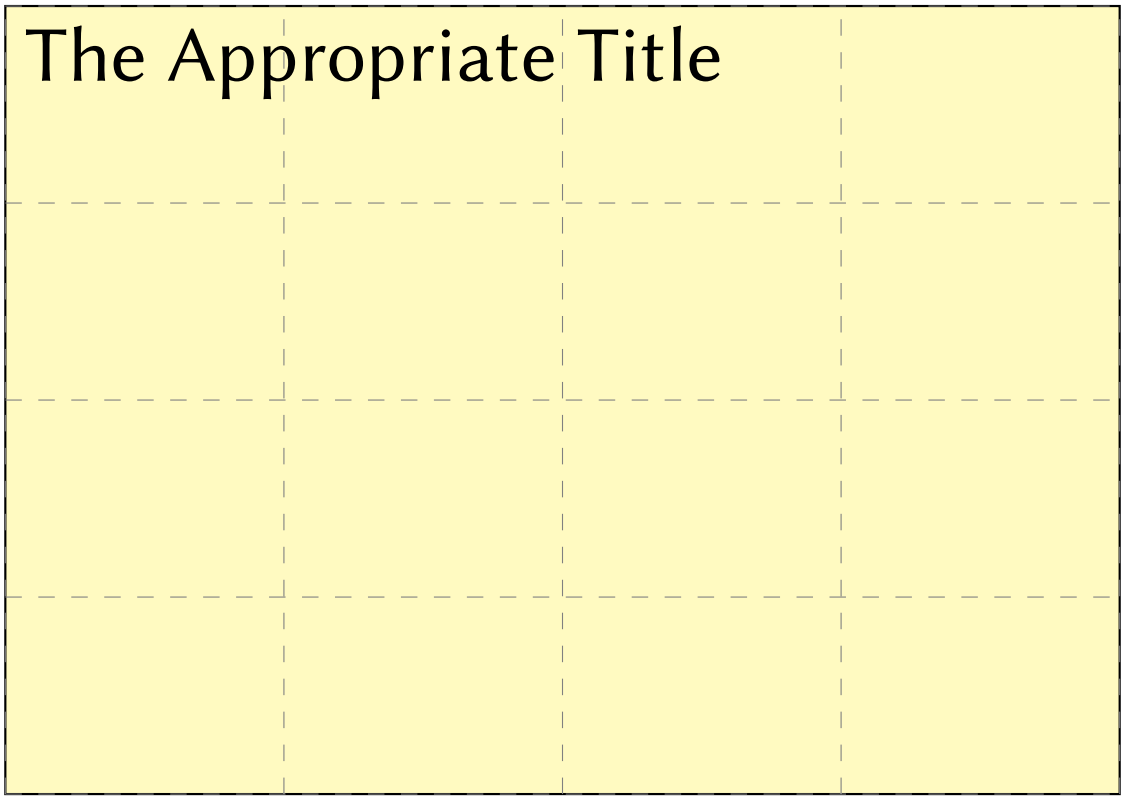

Adjust line separation

\linespread{0.8}

Fall in love with some activity, and do it! Nobody ever figures out what life is all about, and it doesn't matter. Explore the world. Nearly everything is really interesting if you go into it deeply enough. Work as hard and as much as you want to on the things you like to do the best. Don't think about what you want to be, but what you want to do. Keep up some kind of a minimum with other things so that society doesn't stop you from doing anything at all.

R. Feynman

\linespread{1.3}

Fall in love with some activity, and do it! Nobody ever figures out what life is all about, and it doesn't matter. Explore the world. Nearly everything is really interesting if you go into it deeply enough. Work as hard and as much as you want to on the things you like to do the best. Don't think about what you want to be, but what you want to do. Keep up some kind of a minimum with other things so that society doesn't stop you from doing anything at all.

Divide text into paragraphs

Fall in love with some activity, and do it! Nobody ever figures out what life is all about, and it doesn't matter. Explore the world. Nearly everything is really interesting if you go into it deeply enough. Work as hard and as much as you want to on the things you like to do the best. Don't think about what you want to be, but what you want to do. Keep up some kind of a minimum with other things so that society doesn't stop you from doing anything at all.

Fall in love with some activity, and do it! Nobody ever figures out what life is all about, and it doesn't matter.

Explore the world. Nearly everything is really interesting if you go into it deeply enough. Work as hard and as much as you want to on the things you like to do the best. Don't think about what you want to be, but what you want to do.

Keep up some kind of a minimum with other things so that society doesn't stop you from doing anything at all.

Adjust line length

Fall in love with some activity, and do it! Nobody ever figures out what life is all about, and it doesn't matter.

Explore the world. Nearly everything is really interesting if you go into it deeply enough. Work as hard and as much as you want to on the things you like to do the best. Don't think about what you want to be, but what you want to do.

Keep up some kind of a minimum with other things so that society doesn't stop you from doing anything at all.

Adjust line length

Fall in love with some activity, and do it! Nobody ever figures out what life is all about, and it doesn't matter.

Explore the world. Nearly everything is really interesting if you go into it deeply enough. Work as hard and as much as you want to on the things you like to do the best. Don't think about what you want to be, but what you want to do.

Keep up some kind of a minimum with other things so that society doesn't stop you from doing anything at all.

Use Appropriate Colors

Use high contrast colors, like black on a light color.

Avoid green on other ligths.

Try to use emphasis moderately, as multiple emphasized words only **cause loss** of attention, complicate the comprehension and look awful.

Do not fill background.

Use high contrast colors, like black on a light color.

Avoid green on other ligths.

Try to use emphasis moderately, as multiple emphasized words only cause loss of attention, complicate the comprehension and look awful.

Do not fill background.

Zeroth rule of typography

You can break any rule as long as you are aware of it

Outline

bit.ly/upol-posters

Conclusions

The poster is your way
to convey your message

Message

Be able to grab the attention

Provide necessary introduction

Supplement the needed details

Text and Graphics

Work on graphical parts

Make the poster readable

bit.ly/upol-posters

Conclusions

The poster is your way
to convey your message
with help of text and graphics

Message

- Be able to grab the attention
- Provide necessary introduction
- Supplement the needed details

Text and Graphics

- Work on graphical parts
- Make the poster readable

bit.ly/upol-posters

Conclusions

The poster is your way
to convey your message
with help of text and graphics

to the people who came to grab a beer

Message

- Be able to grab the attention
- Provide necessary introduction
- Supplement the needed details

Text and Graphics

- Work on graphical parts
- Make the poster readable

bit.ly/upol-posters

Last Minute Checklist

Images do not pixelate on zooming in

Text is readable (font sizes are appropriate)

Spelling is correct

bit.ly/upol-posters